

KU LEUVEN

 **FACULTEIT
INGENIEURSWETENSCHAPPEN**



**Politecnico
di Torino**

Exploiting electrochemical biosensing strategies for ethanol determination in yeast fermentation

Caterina Marchetti

Thesis submitted to
obtain the degree of Master
of Science in Biomedical Engineering,
option Biomedical instrumentation

Thesis supervisor:
Prof. Irene Taurino
Prof. Danilo De Marchi

Academic year 2024-2025

© Copyright by KU Leuven

Without written permission of the supervisor(s) and the authors it is forbidden to reproduce or adapt in any form or by any means any part of this publication. Requests for obtaining the right to reproduce or utilize parts of this publication should be addressed to KU Leuven, Faculty of Engineering Science - Kasteelpark Arenberg 1, B-3001 Heverlee (Belgium). Telephone +32-16-32 13 50 & Fax. +32-16-32 19 88.

A written permission of the supervisor(s) is also required to use the methods, products, schematics and programs described in this work for industrial or commercial use, and for submitting this publication in scientific contests.

© Copyright by KU Leuven

Zonder voorafgaande schriftelijke toestemming van zowel de promotor(en) als de auteur(s) is overnemen, kopiëren, gebruiken of realiseren van deze uitgave of gedeelten ervan verboden. Voor aanvragen tot of informatie i.v.m. het overnemen en/of gebruik en/of realisatie van gedeelten uit deze publicatie, wend u tot de KU Leuven, Faculteit Ingenieurswetenschappen - Kasteelpark Arenberg 1, B-3001 Heverlee (België). Telefoon +32-16-32 13 50 & Fax. +32-16-32 19 88.

Voorafgaande schriftelijke toestemming van de promotor(en) is eveneens vereist voor het aanwenden van de in dit afstudeerwerk beschreven (originele) methoden, producten, schakelingen en programma's voor industrieel of commercieel nut en voor de inzending van deze publicatie ter deelname aan wetenschappelijke prijzen of wedstrijden.

Foreword

It is with these words that my university journey as a student ends. These years in Politecnico and the year spent in Leuven formed me into the person I am today.

First, I want to thank Irene for the opportunity she gave me to write this thesis under her supervision. It was such an immense pleasure working for such an impressively prepared Professor like herself. The work I did in the lab in Leuven has been a wonderful occasion to better get to know myself and my skills and understand what future path I want to follow. Moreover, working with very skilled persons such as Nurul, Mitty, Filippo, Catarina and Batist gave me a beautiful and hopeful view of the future of research.

Next, I want to thank my parents for being by my side all these years, giving me their full unwavering support. I can easily say that I could not have done it without them. Words fail me in expressing my gratitude towards them and what they mean to me, they are my light.

A big thank you to Sebastian, my wonderful partner who stood next to me in the last year and a bit, even if it seems as though he has been next to me for an entire life already. He lived my struggles during this intense last year and not once did he ever give up on me. Thank you, my love, for being who you are.

I want to thank my aunts and uncles, and also my beloved grandparents, who are looking down at me proudly from above.

Finally, I would like to thank all my friends. I am so lucky to be able to call so many people friends. Among them there are people I bring with me since I was a little kid, and some that I encountered along the way but left a big mark in my life. Grazie Marti, Ceci, Dema, Schael and all the others that know how much they mean to me.

Table of Contents

Foreword	i
Table of Contents	ii
Abstract	iv
List of figures and tables	vi
1.1 List of figures.....	vi
1.2 List of tables.....	ix
List of abbreviations and symbols	x
Chapter 1: Introduction	1
1.1 Importance of ethanol detection.....	1
1.2 Ethanol sensing.....	2
1.3 Outline of the thesis.....	2
Chapter 2: State of the art for ethanol sensors	4
2.1 Electrochemical sensors.....	4
2.1.1 Types of electrochemical sensors.....	5
2.1.2 Three-electrode setup.....	6
2.1.3 Electrochemical techniques.....	8
2.2 Enzymatic ethanol sensors.....	10
2.2.1 Enzymes for ethanol detection.....	10
2.2.2 AOX based sensors based on O ₂ detection.....	11
2.2.3 AOX based sensors based on H ₂ O ₂ detection.....	11
2.2.3.1 Use of electrocatalysts, mediators, and additional enzymes.....	12
2.2.3.2 Immobilization techniques and fabrication of the electrodes.....	14
2.3 Non-enzymatic ethanol sensors.....	19
2.3.1 Ethanol oxidation reaction on platinum.....	19
2.3.2 Influencing factors on EOR.....	20
2.3.3 Additional elements influencing the EOR.....	21
2.3.4 Nanostructuring of the electrodes.....	22
2.4 Conclusion.....	27

Chapter 3: Experimental work: Enzymatic sensor	28
3.1 Electrode modification.....	28
3.1.1 Materials and methods	28
3.1.2 Immobilization protocol.....	29
3.2 Performance evaluation	30
3.3 Summary and contributions.....	31
Chapter 4: Electrode nanostructuring and pre-screening	33
4.1 Materials and methods	33
4.2 Characterization of the nanostructured electrodes	36
4.2.1 Morphological characterization	36
4.2.2 Evaluation of electroactive area and roughness factor	36
4.2.3 Performance evaluation	38
4.3 Summary and contributions.....	40
Chapter 5: Sensing of ethanol in neutral environment	41
5.1 Materials and methods	41
5.2 Definition of the optimal potential window in CV.....	42
5.3 Identification of ethanol electrooxidation peaks in CV.....	45
5.3.1 Determination of the calibration potential in CA	46
5.3.2 Calibration in CA.....	47
5.4 Interference study.....	48
5.4.1 Glucose cross-interference analysis	49
5.5 Summary and contributions.....	51
Chapter 6: Sensing of ethanol in acidic environment	52
6.1 Materials and methods	52
6.2 Definition of the optimal potential window in CV.....	54
6.3 Identification of ethanol electrooxidation peaks in CV.....	57
6.3.1 Glucose cross-interference with ethanol detection in CV.....	58
6.4 Sensor's calibration using CA	60
6.5 Intra-electrode reproducibility	62
6.6 Sensor's calibration.....	63
6.7 Summary and contributions.....	64
Chapter 7: Conclusion and future works	65
Bibliography	68

Abstract

Ethanol detection is crucial in many research and application fields. Among these the pharmaceutical, clinical and food and beverage industries rely on the quantification of ethanol in fluids. In the pharmaceutical and clinical field, ethanol is detected in biological fluids such as blood, sweat, interstitial fluid and breath. In the food and beverage industry, ethanol detection is fundamental to produce alcoholic beverages. The yeast fermentation process is at the base of alcoholic beverages and other food products.

In addition to ethanol, both biological fluids and alcoholic beverages contain glucose. Therefore, it is of great research interest to understand how the detection of ethanol is affected by the presence of glucose.

The detection of analytes in solution is generally performed using bulky, expensive and operator-dependent instrumentation. Electrochemical sensors are considered a good alternative to the classic methods as they are portable, less expensive and are characterized by a good sensitivity and low limit of detection (LoD).

These sensors are classified in two categories: enzymatic and non-enzymatic. In this thesis both solutions have been investigated by developing Pt-based electrochemical sensors.

The significant results of this work are: (i) the effective nanostructuring of Pt screen printed electrodes to enhance the detection performance of the sensor. The roughness factor obtained, which measures the increase of the sensing area, is around 120; (ii) the effective ethanol detection in chloride-free neutral and acidic solution, with and without glucose using non-enzymatic sensor. The sensors exhibited a linear response in the range 0 – 10 mM ethanol ($R^2 > 0.96$). These concentrations of ethanol characterize diluted alcoholic beverages. The sensitivity of the sensor in neutral environment in the absence of glucose resulted to be $145 \pm 7 \text{ uA}/(\text{mM}\cdot\text{cm}^2)$ with a LoD of $849 \pm 43 \text{ uM}$. In acidic environment the ethanol sensitivity was tested in solutions with different glucose concentrations. The sensing conditions that gave rise to the best ethanol

detection performance is in the absence of glucose, in which the sensitivity resulted to be $274 \pm 17 \text{ uA}/(\text{mM} \cdot \text{cm}^2)$ with a LoD of $1130 \pm 70 \text{ uM}$.

List of figures and tables

1.1 List of figures

Figure 2.1: a) Representation of three electrodes set up, b) representation of silver/silver chloride RE, c) screen printed electrodes with WE and CE in carbon (110), gold (220) and platinum (550) [18]	8
Figure 2.2: Cyclic voltammetry technique. (a) voltage-time graph, (b) voltammogram.....	9
Figure 2.3: Scheme of reactions involved in ethanol sensing by AOX via (a) direct, (b) indirect detection of H ₂ O ₂ . Figure taken from [2].....	12
Figure 2.4: Scheme of reactions involved in ethanol sensing via AOX with (a) mediated electron transfer. Schemes (b) and (c) represent the mechanisms of detection of bienzymatic biosensors. Figure adapted from [2]	13
Figure 2.5: Scheme of direct electron transfer based electrodes. Figure adapted from [2]	14
Figure 2.6: EOR mechanisms on Pt catalyst. Figure adapted from [40]	19
Figure 2.7: Scheme of ethanol concentration influence on the EOR	20
Figure 3.1: Photos of the modified SPE with the enzyme Hansenula. In a) and b) the electrode on the left is prepared by including 9mg of enzyme, the one on the right 2mg. a) 24 hours after the deposition; b) Zoomed-in view of the sensing area.....	31
Figure 3.2: CA response of Hansenula electrodes in 0.1 M PBS with consecutive ethanol spike. Stirring rate: 300 rpm; applied potential: 0.7 V vs Ag/AgCl RE	31
Figure 4.1: Representation of a CV scan in H ₂ SO ₄ after nanostructuring. The red rectangle represents the electrochemical double layer current density.....	35

Figure 4.2: SEM images of the nanostructured electrodes. a) Result of CC electrodeposition,.....	36
Figure 4.3: Comparison of CV scans in 0.5 M H ₂ SO ₄ before and after electrodeposition. a) CV scan of CC nanostructured electrodes (blue) and bare Pt electrodes (red), b) CV scan of LSV nanostructured electrodes (blue) and bare Pt electrodes (red), c) Zoom in of CV scan of bare Pt electrodes. Scan rate: 100 mV/s.	37
Figure 4.4: Comparison of bare SPE and nanostructured SPE in different environments in the absence and presence of 0.5 M of ethanol. (a) CV in 0.1 M chloride-free PBS (pH 7); (c) CV in 0.5 M H ₂ SO ₄ ; (e) CV in 1 M KOH. (b), (d) Zoom ins of bare SPE in the neutral and acidic environment respectively. Sample size in (a), (b) n = 3. Scan rate: 100 mV/s.....	39
Figure 5.1: CV measurements to identify the lower potential of the window in 0.1 M chloride-free PBS (pH 7) without (a), and with 2.5 mM ethanol (b). Scan rate: 25 mV/s.	43
Figure 5.2: CV measurements to identify the upper potential of the window in 0.1 M chloride-free PBS (pH 7) without (a), and with 2.5 mM ethanol (b). Scan rate: 25 mV/s.	44
Figure 5.3: CV acquired for different concentrations of ethanol in the range 0-10 mM at nanostructured electrodes in 0.1 M chloride-free PBS (pH 7). Oxidation peak I) and reduction peak II) are more prominent as the ethanol concentration increases. Scan rate: 25 mV/s.....	45
Figure 5.4: Time-current response to the addition of 2.5 mM ethanol at different applied potentials for electrode 1 (a), and 2 (b) in 0.1 M chloride-free PBS (pH 7). (c) CA average step current at different applied potentials; error bars: standard error of the step current for three electrodes. Sample size: n=3; stirring speed: 600 rpm.....	46
Figure 5.5: CA response to ethanol in 0.1 M chloride-free PBS (pH 7). (a) Time-current graph with ethanol additions every 100 s; (b) Average calibration curve; error bars: standard deviation among three electrodes. Sample size: n=3; stirring speed: 600 rpm; applied potential: 0 V vs Ag/AgCl RE.....	47
Figure 5.6: CA interference study in 0.1 M chloride-free PBS (pH 7). (a) Time-current plot with additions every 100 s; (b) Zoom in of (a). Sample size n=3; stirring speed: 600 rpm; applied potential: 0 V vs Ag/AgCl RE.	48
Figure 5.7: CV analysis of cross-interference analysis between glucose and ethanol in 0.1 M chloride-free PBS (pH 7). Medium containing increasing concentrations of ethanol between 0 and 10 mM and: (a) 1 mM glucose, (b) 5 mM glucose, (c) 10 mM glucose. Oxidation peaks I and II are proportional with ethanol concentrations. Scan rate: 25 mV/s.	51

Figure 6.1: CV measurements to identify the lower potential of the window in 0.1 M chloride-free PBS (pH 4) without (a), and with 2.5 mM ethanol (b). Scan rate: 25 mV/s.....55

Figure 6.2: CV measurements to identify the higher potential of the window in 0.1 M chloride-free PBS (pH 4) without (a), and with 2.5 mM ethanol (b). Scan rate: 25 mV/s.....56

Figure 6.3: CVs acquired for different concentrations of ethanol in the range 0-10 mM at nanostructured electrodes in 0.1 M chloride-free PBS (pH 4). Oxidation peaks I) and II) are more prominent as the ethanol concentration increases. Scan rate: 25 mV/s.....57

Figure 6.4: CVs in absence and presence of 5 mM ethanol in 0.1 M PBS (pH 4) in the presence of chlorides. Scan rate: 25 mV/s.....58

Figure 6.5: Qualitative analysis of ethanol and glucose cross interference in 0.1 M chloride-free PBS (pH 4). (a) CVs at two different concentrations of glucose (2.5 and 7.5 mM) in the presence of ethanol (5 mM). (b) CVs at two different concentrations of ethanol (2.5 and 7.5 mM) in the presence of glucose (5 mM). Peak I) and II) are representative of ethanol oxidation. Scan rate: 25 mV/s.....59

Figure 6.6: Average step current response to 2.5 mM ethanol (a) and 2.5 mM glucose (b) in 0.1 M chloride-free PBS (pH 4) at different potentials. (a) Continuous CA protocol for ethanol measurements; error bars: standard error of the step current for three electrodes. Sample size: n=3; stirring speed: 450 rpm. (b) Spiking CA protocol for glucose measurements; error bars: standard error of the step current for two electrodes. Sample size: n=2; stirring speed: 600 rpm.....61

Figure 6.7: CVs in 0.1 M chloride-free PBS (pH 4) containing 10mM ethanol of the same electrode used three consecutive times. Scan rate: 25 mV/s.....62

Figure 6.8: CV scans in 0.1 M chloride-free PBS (pH 4) with different ethanol concentrations after baseline subtraction. The peak currents were identified manually. Scan rate: 25 mV/s64

1.2 List of tables

Table 2.1: List of enzymatic ethanol sensors, with focus on the yeast species used, the electrode, the enzyme immobilization technique and the sensing performance (sensitivity, LoD and linear range of detection). In blue are highlighted the immobilization methods, in green the mediators, in orange the electrocatalysts and in purple the presence of the second enzyme HRP.	16
Table 2.2: List of non-enzymatic ethanol sensors, with focus on the electrodes used, the geometric area and the ESA, the nanostructuring technique, the analysis media and the sensing performance (sensitivity, LoD and linear range). In red are the catalytic elements.....	24
Table 4.1: Comparison between electrodeposition techniques in term of ESA, Rf and applied charge.....	38
Table 6.2: Comparison of ethanol sensitivity and LoD in 0.1 M chloride-free PBS (pH 4)	63

List of abbreviations and symbols

ADH	Alcohol Dehydrogenase
AOX	Alcohol Oxidase
BAC	Blood Alcohol Concentration
BrAC	Breath-analysers Alcohol Concentration
BSA	Bovine Serum Albumin
CC	Chronoamperometry
CC	Chronocoulometry
CE	Counter Electrode
CDI	Carbonyldiimidazole
CV	Cyclic Voltammetry
DEMS	Differential Electrochemical Mass Spectrometry
ESA	Electroactive Surface Area
EOR	Ethanol Oxidation Reaction
FAD	Flavin Adenine Dinucleotide
FTIR	Fourier-Transform Infrared Spectroscopy
GA	Glutaraldehyde
GC	Gas Chromatography
GCE	Glassy Carbon Electrode
GOX	Glucose Oxidase
HER	Hydrogen Evolution Reaction
HPLC	High Performance Liquid Chromatography
HRP	Horseradish Peroxidase
IR	Infrared Spectroscopy
LoD	Limit of Detection
LSV	Linear Sweep Voltammetry
MS	Mass Spectrometry
MSE	Mercury-mercurous Sulphate Electrode
NAD ⁺	Nicotinamide Adenine Dinucleotide
NIR	Near Infrared Spectroscopy
OER	Oxygen Evolution Reaction
PANI	Polyaniline
PB	Prussian Blue
PBS	Phosphate-buffered Saline
PEI	Polyethylenimine

PNR	Poly Neutral Red
pOPD	poly-Ortho-Phenylenediamine
PPY	Polypyrrole
PU	Polyurethane
RE	Reference Electrode
Rf	Roughness factor
SCE	Saturated Calomel Electrode
SEM	Scanning Electron Microscope
SPE	Screen Printed Electrodes
XPS	X-ray Photoelectron Spectroscopy
WE	Working Electrode

Chapter 1: Introduction

1.1 Importance of ethanol detection

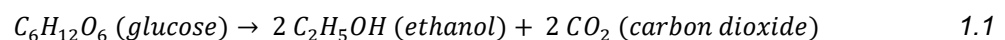
Ethanol detection is an important topic in various fields of research, ranging from the pharmaceuticals, clinical research, food and beverage industries, and ethanol fuel cell research [1], [2].

Different ethanol sensors have been developed for alcohol detection in body fluids, such as breath, sweat, urine and blood. Blood alcohol concentration (BAC) sensors and breath-analysers (BrAC) play a key role in improving road safety by detecting alcohol consumption [3]. Additionally, ethanol detection in biofluids such as sweat, interstitial fluids, tears and saliva is crucial for clinical and forensic analysis [2].

Beyond medical and safety applications, ethanol detection is also crucial for assessing product quality in the food, beverage, and agricultural industries. Moreover, continuous ethanol monitoring is vital in processes such as the fermentation of alcoholic beverages [1], which is the focus of this project.

The fermentation process consists in the metabolism of carbohydrates into alcohols or acids by eukaryotic organisms, such as yeasts. This process is responsible for producing a wide range of products, including beer, wine, cider, yogurt, cheese, bread, and coffee [4].

Ethanol is the main reaction product of glucose metabolism in alcoholic fermentation, as shown by Equation 1.1 [4]:



The most widely used yeast strain for alcoholic fermentation is *Saccharomyces cerevisiae*. In beer production, this yeast converts the sugars present in malted cereals, one of the four ingredients needed to produce beer, into ethanol and carbon dioxide [4]. Monitoring ethanol levels throughout fermentation is essential to ensure process control and maintain the quality of the final product.

1.2 Ethanol sensing

Conventional methods for ethanol sensing are chromatography and spectroscopy.

Chromatography is a separation technique that is carried out exploiting either the different sizes of the chemical compounds, electrostatic interactions or affinity tendencies [5].

Spectroscopy includes various techniques such as mass spectrometry (MS), near infrared spectroscopy (NIR), Raman spectrometry. These techniques determine analyte concentration by analysing its interaction with electromagnetic waves.

While both methods are highly precise and reliable, they are characterized by a bulky, expensive, complex and operator-dependent instrumentation. Due to these limitations, these techniques are unsuitable for *in situ*, continuous, real-time measurements, which are essential for processes like fermentation. To address this issue, the past two decades have seen the development of more portable and cost-effective ethanol sensors [1]. Among the various chemical sensors used for this purpose, electrochemical sensors stand out for their good sensitivity and low limit of detection [6].

Electrochemical sensors are classified into two categories: enzymatic and non-enzymatic. The strong aspects of one category are the weak aspects of the other category. In particular, enzymatic sensors are characterized by high selectivity but are affected by numerous issues such as the influence of the environment (pH, temperature and humidity) on the activity of the enzymes, short enzyme lifespan, inefficient electron transport between the enzyme and the electrode surface, challenging immobilization techniques, and low reproducibility [7]. On the contrary, the non-enzymatic sensors are more stable, as they are not affected by environmental conditions or enzyme degradation or inefficiency in the electron transport between the enzyme and the electrode surface. However, they suffer from lower selectivity and are prone to poisoning effects. In fact, intermediates and byproducts of the reactions occurring on the electrode, as well as interferents and chloride ions tend to adsorb onto the electrode surface, reducing the catalyst's sensing performance [7].

1.3 Outline of the thesis

This thesis focuses on the development of a platinum-based ethanol sensor for continuous monitoring of ethanol.

Chapter 2 provides an overview of electrochemical sensors and techniques, followed by a review of the state of the art of enzymatic and non-enzymatic electrochemical ethanol sensors. The enzymatic sensors developed in literature differ based on the enzyme used, the species of the enzyme, the immobilization procedures, and the addition of elements that enhance the performance of the electrode. Non-enzymatic ethanol sensors in literature differ based on the composition of the catalyst and the nanostructuring of the electrode.

Chapter 3 details the development of the enzymatic sensor, including the choice of enzyme species and immobilization techniques. This is followed by the description and analysis of the experimental work that was conducted to investigate the sensor's performance. Chapter 4, 5 and 6 focus on the non-enzymatic sensor.

Chapter 4 details the nanostructuring of electrodes using two different techniques and comparing their effectiveness. An ethanol pre-screening analysis is also performed in all pH environments.

Chapter 5 and 6 present the experiments conducted on the nanostructured electrodes in neutral and acidic environments, respectively. These two chapters also examine the cross-interference between glucose and ethanol, as both analytes are present in the beer fermentation broth. This has been considered as the principal application of this work.

Finally, Chapter 7 summarizes the conclusions of the study and outlines potential future research directions.

Chapter 2: State of the art for ethanol sensors

The conventional methods for ethanol detection include chromatography (e.g. high-performance liquid chromatography (HPLC), gas chromatography (GC)), spectroscopy (e.g. Fourier-transform infrared spectroscopy (FTIR), infrared spectroscopy (IR)) and spectrometry (e.g. mass spectrometry (MS)) [1]. While these methods are precise and reliable, they are also complex, operator-dependent, bulky, and expensive [1]. In contrast, electrochemical sensors provide a portable, cost-effective, and user-friendly alternative for on-site, real-time ethanol measurements.

2.1 Electrochemical sensors

Chemical sensors, as defined by IUPAC [8], are devices capable of transforming chemical information, such as ethanol concentration, into an analytical signal. Every chemical sensor comprises two functional units: a receptor and a transducer. The receptor is responsible for the transformation of chemical information into a form of energy, which the transducer then transforms into an analytical, readable signal [8].

Chemical sensors can be classified based on the transducer's physical principle, including optical, electrochemical, electrical, mass sensitive, magnetic, and thermometric sensors [8]. The **electrochemical sensors** are defined by IUPAC as devices that: “[...] transform the effect of the electrochemical interaction analyte - electrode into a useful signal” [8]. These sensors are characterized by high working speed, low limit of detection, and good sensitivity, making them highly attractive for analyte detection [6].

The main characteristics of electrochemical sensors include the following.

- I. Selectivity. The ability to recognise the target analyte without interference from other species. A selective sensor can sense other substances but it

“exhibits a degree of preference for the substance of interest” [9]. Selectivity is often assessed by testing the sensor in a solution containing possible interferents. An important issue in electrochemical sensors is fouling, the gradual formation of a non-conductive layer of organic species on the surface of the electrode, which can severely hamper the performance of the sensor [10].

- II. Specificity. The ultimate, or ideal form of selectivity, the ability to recognise only the target analyte. The contribution to the result of a specific sensor comes only from the target analyte and no other components [9].
- III. Sensitivity. The extent to which the output signal changes with the variation in the target analyte concentration [10]. This is usually evaluated by measuring the sensor’s response to known concentrations of the target analyte.
- IV. Limit of detection (LoD). The measure of the lowest detectable analyte concentration [10]. Concentrations of analyte lower than the LoD cannot be distinguished from background noise. Therefore, the LoD is usually computed as three times the signal to noise ratio.
- V. Stability. The ability to preserve the signal over time [10]. Stability is measured in two ways: the operational and the storage stability. The first is the ability of the sensor to retain a stable signal over time while continuously measuring the concentration of the target analyte [11]. The second is the ability of the sensor to maintain the original sensitivity to the target analyte after being stored in the right conditions for a certain amount of time [11].
- VI. Repeatability. The ability to obtain consistent results across multiple experiments conducted using the same method, the same test material and under the same conditions [12].
- VII. Reproducibility. The ability to obtain consistent results across multiple experiments conducted using the same method, the same test material under different conditions [13].
- VIII. Linear range. The concentration range over which the output signal is directly proportional to the analyte molarity [14]. It is measured using the Pearson correlation index [10]. A sensor with a wide linear range can be used to detect a broad range of analyte concentrations.

2.1.1 Types of electrochemical sensors

Electrochemical sensors can be categorized in amperometric, potentiometric, and conductometric/impedimetric [15].

- I. The **amperometric** sensors’ working principle is based on the application of a voltage between the electrode at which the analyte is detected, also

called working electrode (WE), and the reference electrode (RE), which acts as a stable reference potential [15]. The application of the potential induces oxidation or reduction of the desired electroactive species, which results in a continuous flow of electrons between the electrodes and therefore a continuous measurement of current [15]. The potential applied can be constant or variable. In the first case the measurement method is called amperometry, in the latter case voltammetry. In these sensors the peak current value that is measured is directly proportional to the concentration of the analyte present in the solution [15]. The sensitivity that characterises these sensors is expressed in ampere/molar.

- II. **Potentiometric** devices measure the potential difference between the WE and the RE when no current is allowed to flow between them. These sensors are typically used to determine ion concentrations in a solution, such as in pH measurement [15].
- III. The **conductometric** or **impedimetric** sensors measure the surface impedance as it changes when the analyte molecules bind to specific binding elements on the electrode surface [6].

2.1.2 Three-electrode setup

Amperometric sensors typically use a **three-electrode setup**, comprising a working electrode (WE), a counter (or auxiliary) electrode (CE) and a reference electrode (RE), all submerged in an electrolyte (Figure 2.1 (a)). These electrodes are then connected to a potentiostat which is the instrument that allows for the control of the potential applied to the electrodes, as well as for the measurement of the output current.

The **WE** is made out of receptor and transducer. The chemical reaction that causes the detection of the analyte takes place on the receptor's surface [15]. The analyte undergoes a redox reaction on the WE surface, releasing or accepting electrons.

The **RE** provides a stable applied potential difference [15]. Common REs include silver/silver chloride (Ag/AgCl), saturated calomel electrode (SCE), and mercury-mercurous sulphate electrode (MSE). These electrodes are chosen for their high reproducibility and stability.

The Ag/AgCl electrode consists of a silver wire in contact with AgCl in a saturated KCl solution (Figure 2.1 (b)). The half-cell reaction at this electrode is the following:



As the cathode a reduction of AgCl takes place forming solid Ag and chloride ions in solution. As an anode the oxidation of Ag occurs: chloride ions release electrons and form solid AgCl. The potential stability of this electrode is achieved by having the saturated KCl as inner filling solution.

It must be taken into consideration that the KCl solution can leak into the electrolyte in which the RE is submerged, therefore some chloride ions can be unwantedly found in solution. For this reason, double junction electrodes can be used. These electrodes have in fact an additional second solution placed between the KCl solution and the electrochemical cell solution in which the analyte is contained [16]. Ag/AgCl RE is the most used in electrochemical settings due to the toxicity of SCE and MSE electrodes.

The SCE electrode is composed of mercurous chloride cathode (Hg_2Cl_2), also called calomel, in contact with a liquid mercury anode (Hg), in saturated KCl solution [16].

The MSE consists of the contact between mercurous sulphate (Hg_2SO_4) and mercury wire (Hg), in a solution of sulphuric acid (0.5 M H_2SO_4) [17].

The **CE** allows for the current to flow from or to the WE when the analyte is respectively reduced or oxidised on the electrode surface [15]. The presence of this electrode prevents any possible impairment of the stability of the RE's potential due to the passage of current.

Therefore, the potentiostat always measures the current that flows between the WE and the CE, whilst the potential is always applied between the WE and the RE [15].

The WE can be manufactured in house for instance by depositing a conductive thin film or by printing a thin layer of conductive inks onto ceramic or plastic substrates creating printed electrodes. Alternatively, electrodes can be bought and modified to adapt them to the wanted application. Among the commercially available electrodes, screen printed electrodes (SPE) are a cheap, easy to use and disposable option for electrochemical sensing. Moreover, the dimensions of these electrodes are less than 4 cm^2 , therefore they can be used with low volumes of sample [18]. These electrodes are manufactured by printing conductive inks onto ceramic or plastic substrates. SPEs integrate a three-electrode cell design, therefore there is no need for the use of external electrodes. The WE can be in platinum, carbon, silver, gold and other materials, while the RE is usually printed Ag/AgCl (Figure 2.1 (c)) [19].

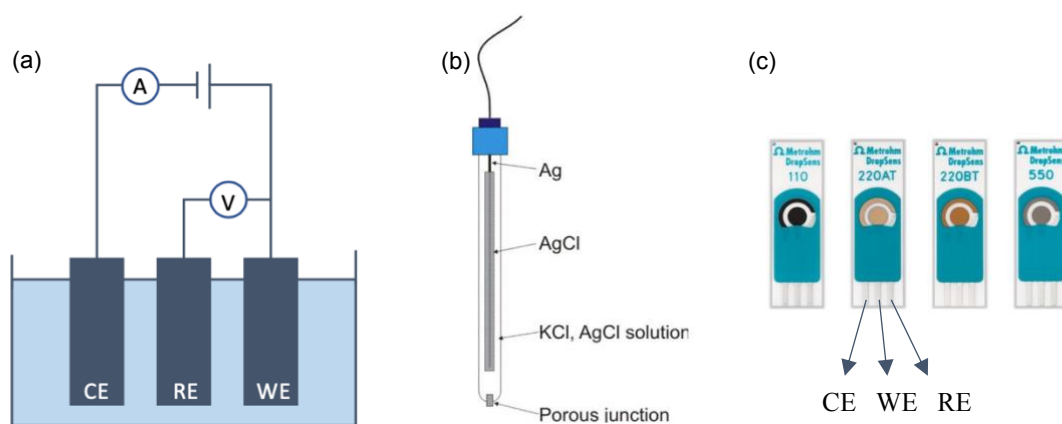


Figure 2.1: a) Representation of three electrodes set up, b) representation of silver/silver chloride RE, c) screen printed electrodes with WE and CE in carbon (110), gold (220) and platinum (550) [18]

2.1.3 Electrochemical techniques

Amperometric techniques, such as voltammetry and chronoamperometry, are commonly used to evaluate the ability of an electrode to sense an analyte. The output current measured is, in fact, proportional to the analyte concentration.

Voltammetry consists in applying a variable potential to the WE and measuring the resulting flow of electrons as generated current [15]. If the voltage is swept cyclically between two potentials, called lower limit potential (E_1 in Figure 2.2) and upper limit potential (E_2 in Figure 2.2), the technique is called cyclic voltammetry (CV), otherwise it is called linear sweep voltammetry (LSV). There are other voltammetric techniques developed to minimize the influence of the capacitive current on the voltammogram. However, the explanation of these methods falls outside the scope of this section, as we will focus only on the techniques employed in the experimental section.

An important parameter that characterises both CV and LSV is the scan rate, which is the ratio between the potential range ($E_2 - E_1$) and the duration of the scan. In Figure 2.2, the scan rate is indicated as $(E_2 - E_1)/(t_2 - t_1)$. This parameter is crucial because, if it results to be too high, there is not enough time for the reactions to occur, for electrons to be exchanged at the electrode surface, therefore, no meaningful information can be extracted from the measurements [15]. In voltammetry, the solution in which the measurement is conducted is generally not stirred, therefore, the only mass transport present is the diffusion.

- I. CV is typically used to identify the potentials at which the oxidation and reduction of chemical compounds happen. The graph in which the measurements are plotted is called voltammogram and has a typical “duck” shape, as can be noticed in Figure 2.2 (b) [15]. The cycle starts from E_1 and proceeds towards E_2 in what is called the forward scan. As the potential increases the compounds in solution diffuse towards the

electrode surface and get oxidised, therefore they lose electrons which give rise to an anodic current. The potential at which the current is maximal is the oxidation potential of the compound ($E_{p,c}$ in Figure 2.2 (b)). As the potential increases further, the current decreases because there are less and less molecules close to the electrode-electrolyte interface that can be oxidised. On the contrary, as the potential is reversed and decreased from E_2 to E_1 , the reduction of the oxidised compounds occurs, therefore electrons are now accepted by the analyte in solution and the current is cathodic [10], [15]. The anodic and cathodic peak current values are proportional to the concentration of analyte present in solution; therefore, this technique can also be used to build the calibration plot and compute the sensitivity of the sensor [10], [15].

- II. LSV is usually implemented to construct the calibration plot for an analyte as the output peak current is proportional to the target's concentration. The principles governing this technique are the same as the ones mentioned for CV.

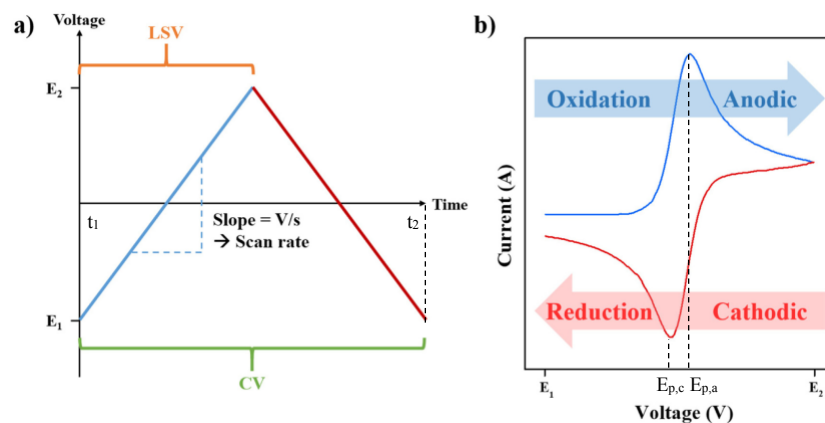


Figure 2.2: Cyclic voltammetry technique. (a) voltage-time graph, (b) voltammogram. Adapted from [20]

Chronoamperometry consists in measuring the current over time when a square-wave voltage is applied between the WE and RE. During this measurement, the solution is generally stirred to keep the diffusion layer constant, therefore guaranteeing a stable output current per each concentration of the target analyte in solution. This technique is very accurate and more used for quantitative analyses and the construction of calibration plots in respect to voltammetry [10], [15].

Amperometric electrochemical sensors can be differentiated into two categories: enzymatic sensors and non-enzymatic ones. In the next two subchapters there is the description of the state of the art for both types of electrodes to sense ethanol.

2.2 Enzymatic ethanol sensors

Enzymatic sensors are based on the activity of biological components that are embedded on the WE. Enzymes are defined as catalysts or catalytic proteins as they have the ability of increasing the rate of chemical reactions for specific substrates. For ethanol detection, two enzymes are widely used: alcohol dehydrogenase (ADH) and alcohol oxidase (AOX). Both are responsible for the oxidation of alcohols into their corresponding aldehydes; therefore, they are also called redox enzymes [2], [15].

2.2.1 Enzymes for ethanol detection

Alcohol dehydrogenase (**ADH**) catalyses the oxidation of primary aliphatic and aromatic alcohols in the presence of the cofactor nicotinamide adenine dinucleotide (NAD^+), as shown in Equation 2.2 [1]:



Sensors incorporating ADH on the WE are highly stable and specific to ethanol. However, the need for the additional cofactor makes this approach less attractive for continuous, real-time measurements [2].

The **AOX** is an octameric protein that includes in its three-dimensional structure the cofactor flavin adenine dinucleotide (FAD). This strongly bound cofactor eliminates the need for additional components for the reaction to occur except for oxygen (O_2), which acts as the electron acceptor [2]. Equation 2.3 shows the ethanol oxidation reaction catalysed by AOX:



To measure the rate at which the reaction above occurs, the sensors need to detect the decrease of O_2 concentration or the increase of hydrogen peroxide (H_2O_2) concentration [2], therefore another distinction of ethanol enzymatic sensors based on AOX is done in the next section.

AOX promotes the oxidation of all short-chain aliphatic alcohols. AOX is produced by methylotrophic yeasts, which are single cell microorganisms that use this enzyme for the methanol oxidation process [2]. For this reason, to prevent the oxidation of low molecular weight alcohols, many ethanol sensors have been developed by including ADH, instead of AOX [2]. On the other hand, considering the application of the sensors to detect ethanol in alcoholic beverages, the concentration of other alcohols can be neglected as compared to the one of the desired analyte. Therefore, AOX based sensors are preferred

to ADH based ones as there is no need for the addition of any cofactor. For this reason, from now on the focus will be on the AOX based sensors.

2.2.2 AOX based sensors based on O₂ detection

AOX sensors can be based on the detection of the decrease of oxygen concentration. In particular, the sensors that monitor the consumption of O₂ make use of the basic principle of the Clark-type O₂ electrode, which was invented in 1962 [2]. This sensor consists of a platinum cathode and a silver reference electrode, both immersed in a potassium chloride electrolyte solution and covered by a O₂ semi-permeable membrane [2]. When a negative potential of 600mV is applied to the Pt electrode relative to the RE, the oxidation reaction takes place at the silver anode, as is shown in Equation 2.4, whilst the reduction reaction occurs at the platinum cathode, as shown in Equation 2.5 [2]:



Therefore, when the potential is applied and the reactions take place, a current proportional to the concentration of O₂ can be measured [2].

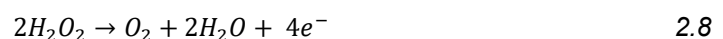
The alcohol oxidase was first included in this sensor by immobilizing it on the cathode through a nylon cloth by Nanjo and Guilbault, in 1975 [1]. These first alcohol sensors are very specific, do not suffer from interferences, but their response, accuracy and reproducibility are very low [2].

2.2.3 AOX based sensors based on H₂O₂ detection

To overcome the disadvantages of the AOX sensors based on O₂ detection, sensors based on the detection of H₂O₂ have been developed in the same period. In particular, the sensing of H₂O₂ can be done by measuring the current that results from the oxidation or reduction of the molecule on the surface of the WE, as shown in Equation 2.6 and 2.7 respectively [2]:



On a platinum WE, when a positive potential of 600mV is applied relative to a Ag/AgCl RE, the oxidation of H₂O₂ yields both H₂O and O₂ as shown in Equation 2.8 [2], [21]:



These sensors are called first generation of biosensors and they allow the direct detection of H₂O₂, as can be seen in Figure 2.3a [2]. Although these sensors are characterized by a wide linear range, the application of such a high voltage

to the WE causes the unwanted oxidation of species normally present in alcoholic beverages, such as ascorbic acid and uric acid, therefore solutions like the addition of electrocatalysts, mediators and additional elements can be implemented to reduce the oxidation potential of H_2O_2 [2].

2.2.3.1 Use of electrocatalysts, mediators, and additional enzymes

To reduce the detection of interferences that characterises the sensors based on the detection of H_2O_2 , a solution is to lower the necessary applied potential. This was achieved by including **electrocatalysts** for either H_2O_2 oxidation or reduction, on the surface of the electrode [2]. These additional compounds, in fact, ease the passage of electrons between the electrode and the transducer element.

The main electrocatalysts used for H_2O_2 reduction are Prussian Blue (PB) and Rhodium, whilst cobalt ions are used for oxidation. This sensing method, which takes the name of indirect H_2O_2 detection, is represented in Figure 2.3 (b) [2]:

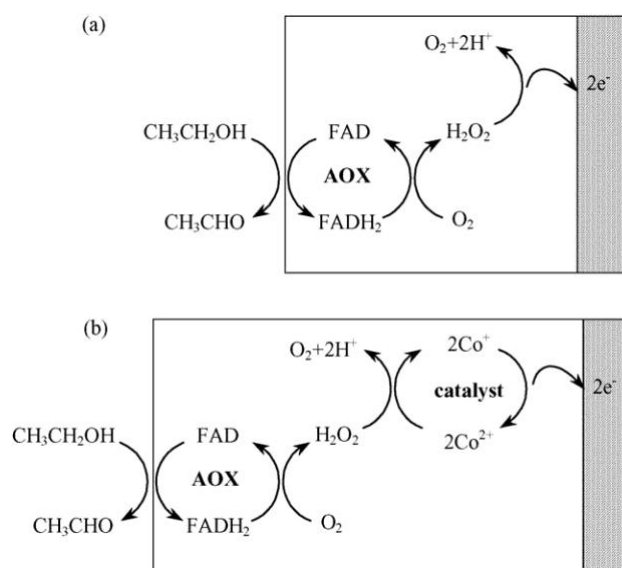


Figure 2.3: Scheme of reactions involved in ethanol sensing by AOX via (a) direct, (b) indirect detection of H_2O_2 . Figure taken from [2]

Another solution to lower interference is to modify the electrode by including **mediators** that act as transporters of electrons between the redox site of the enzyme and the electrode surface [2]. The sensors that include these elements form the so-called second generation of biosensors [2]. Examples of AOX mediators are poly(neutral red) (PNR) [22], cobalt-phthalocyanine (CoPC) [23] or conductive polymers as polyaniline (PANI) [24]. The reaction scheme of this group of sensors is represented in Figure 2.4 (a) [2].

A further solution to solve the interference problem is the addition of a second enzyme, a peroxidase, able to catalyse the reduction of H_2O_2 into H_2O at low potentials [2]. Typically, **bienzymatic** sensors include horseradish peroxidase (HRP) and their working principle can be seen in Figure 2.4 (b).

The last two solutions presented, can be implemented simultaneously to obtain bienzymatic sensors that also include mediators to ease the transfer of electrons between the redox centre in HRP and the electrode surface. The resulting electrodes show higher sensitivity and lower detection limit. Examples of such mediators are ferrocene [25], [26], ferrocyanide [23], polypyrrole (PPY) [27] and Osmium complexes [28]. The reaction scheme is represented in Figure 2.4 (c) [2].

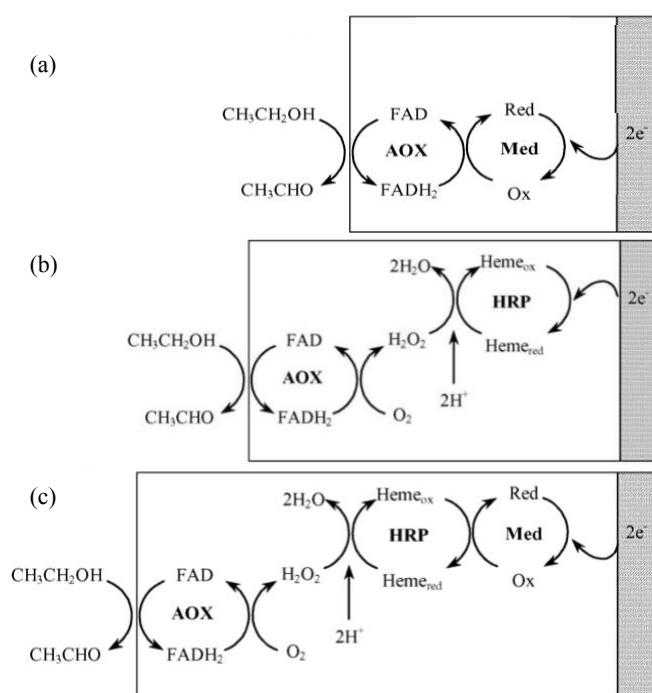


Figure 2.4: Scheme of reactions involved in ethanol sensing via AOX with (a) mediated electron transfer. Schemes (b) and (c) represent the mechanisms of detection of bienzymatic biosensors. Figure adapted from [2]

The main problem that affects the second generation of biosensors is the lack of stability and reproducibility, due to the possible leaching of the mediator and the fact that diffusion of chemical compounds is hampered by these components [29]. Therefore, research is now focused on the third generation of biosensors, which are called **direct electron transfer** sensors. The sensors belonging to this category are characterized by the replacement of O_2 as the electron acceptor [29]. In this way the potential at which the sensor works is closer to the redox voltage of the enzyme and therefore interferences are minimised [29]. Ideally there should be a direct transfer of electrons between the redox centre of AOX and the electrode surface, as can be visualized in Figure 2.5 [2]:

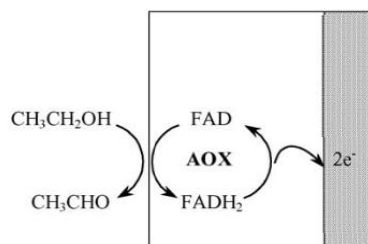


Figure 2.5: Scheme of direct electron transfer based electrodes. Figure adapted from [2]

The main obstacle in the development of such biosensors is the deep embedment of the FAD centre in the AOX enzyme. For this reason, in many projects, the addition of conductive nanostructures was implemented to enhance the electrical communication between the transducer and the FAD centre of the enzyme [1].

2.2.3.2 Immobilization techniques and fabrication of the electrodes

Enzyme immobilization procedures and nanostructuring are techniques that allow to retain a higher quantity of enzyme on the electrode, so that the developed sensors yield a higher response to the target analyte.

Nanostructuring consists in the deposition of nanostructures on the surface of the electrodes to increase their roughness and the surface area. For this reason, higher enzyme quantities can cover the electrode's surface and therefore increase the sensitivity of the sensor [1].

Immobilization techniques are defined as the processes needed to ensure that the enzyme is steadily retained on the surface of the electrode. These methods allow the reaction catalysed by the enzyme to take place as close as possible to the electrode surface, so that the signal is maximised [15]. Nevertheless, precautions need to be taken when immobilizing an enzyme to not cause its denaturation and inactivation [15].

The easiest method to immobilise an enzyme is to use a membrane via **non-covalent entrapment**. The membrane's role can be only supportive, or it can also act as a barrier and prevent interfering components from reaching the electrode surface [2]. For example, nitro-cellulose acetate and polycarbonate membranes were both successfully used as an interference barrier in a study conducted in the 2000 [30]. In another study, poly-ortho-phenylenediamine (pOPD) was used as a perm-selective membrane, whilst polyurethane (PU) was used as outer layer [31]. Other examples of interference barriers used for ethanol sensors are pOPD film, non-conductive overoxidized polypyrrole (PPY_{ox}) film [32], and Nafion [33], [34], [24]. Numerous conductive polymers have been used to retain the enzyme while also enhancing the performances of the electrode. Examples are PPY, PEDOT, PEDOP [35], and polyaniline (PANI)

[34]. In other cases, enzymes can be included in the electrode by mixing a conductive powder with the enzyme solution obtaining an electrode paste [26], [28]. In another application, the entrapment of the enzyme was obtained by including the AOX and HRP enzymes in a calcium alginate hydrogel [36].

Another solution is to **crosslink** the enzyme with a polymer or with other proteins that allows a higher quantity of enzyme to be loaded on the electrode [2]. The most popular crosslinker used is glutaraldehyde (GA), generally coupled with bovine serum albumin (BSA) as can be seen in Table 2.1 [32], [22], [11], [33].

The two immobilization methods just described are affected by the disadvantage of not controlling the orientation of the adsorbed enzyme, which is instead addressed by the immobilization techniques based on **covalent binding** of the enzyme to the electrode [37]. For example, a sensor was created by covalently coupling HRP and AOX with a carbonyldiimidazole (CDI) activated graphite powder. This sensor shows increased stability and sensitivity relative to other sensors prepared without the activation of the graphite powder [28].

In general, the enzyme prepared with these immobilization methods is afterwards deposited on the electrode via techniques, among which the two most popular are drop casting and electrodeposition.

The first method consists in simply pipetting the correct amount of enzyme solution onto the WE surface. This process is followed by a drying period and a subsequent storage of the electrodes in the fridge before usage.

The second method is based on the application of a voltage to the electrode submerged into a solution containing the enzyme. For example, if the enzyme is immobilized using conductive polymers, the solution in which the potential is applied contains the desired monomers and the enzyme [30].

Moving away from immobilization strategies, the increase of the sensor's performance can be obtained by including **nanstructures** on the electrode's surface. In 2015 for example stabilised gold nanoparticles coupled with AOX were dispersed on the surface of a glassy carbon electrode (GCE). This inclusion increased noticeably the sensitivity of the electrode relative to the incorporation of only AOX [34].

Finally, some elements called enzyme stabilizers can be added to the sensor to increase its stability [37]. Examples of stabilizers, that can also be found in Table 2.1, are glycerol [31], lactitol [28], dextrane [28] and polyethylenimine (PEI) [28], [31], [38].

Table 2.1: List of enzymatic ethanol sensors, with focus on the yeast species used, the electrode, the enzyme immobilization technique and the sensing performance (sensitivity, LoD and linear range of detection). In blue are highlighted the immobilization methods, in green the mediators, in orange the electrocatalysts and in purple the presence of the second enzyme HRP.

Year of publication	Type of yeast species (company)	Type of electrode used (area)	Enzyme deposition technique	Sensitivity	Linear detection range (mM)	LoD (mM)
2012 [23]	«Pichia Pastoris «Candida Boidinii «Hansenula sp. (Sigma-Aldrich)	Screen printed carbon electrodes modified with: Prussian Blue (SPPBCE), Ferrocyanide (SPFCE), Co-phthalocyanine (SPCPCE) (0.1256 cm ²)	Drop casting of 10 uL of AOX/HRP mix (0.05 U/uL each) (no HRP included on SPCE/CP).	1.205 uA/mM	0.05 – 1	0.02
2000 [30]	Pichia Pastoris (Sigma-Aldrich)	Screen printed carbon electrode doped with cobalt phthalocyanine (CoPC-SPCE) (0.09 cm ²)	Drop casting of 5 uL of AOX solution. Cover with a membrane of nitrocellulose acetate or polycarbonate	1.201 uA/mM	0.12 – 2	-
2009 [11]	Hansenula sp. (Sigma-Aldrich)	Screen printed Pt electrode	Drop casting of AOX solution with 5% BSA and treatment with GA vapor	~3 nA/mM (deduced from graph)	0.3 – 20	0.3
2017 [31]	Pichia Pastoris (Sigma-Aldrich)	Pt-Ir electrodes covered with pOPD	Dipping the electrode in a mix of AOX in PBS pH=7.4, glycerol, PEI and PU (all 1% sol)	25.4 nA/mM	0 – 10	0.049
2001 [38]	«Hansenula «Candida Boidinii «Pichia Pastoris (Sigma-Aldrich)	Pt screen printed electrode (0.0314 cm ²)	Drop casting of 2uL of the mixture composed by the enzyme solution, PEI and poly(carbamoyl)sulfonate (PCS) prepolymer (to create hydrogel)	30.5 nA/mM 10.6 nA/mM 6.2 nA/mM (HS, PP, CB respectively)	0.01 – 3 0.02 – 3.75 0.04 – 3.75	-

2011 [33]	Pichia Pastoris (Sigma-Aldrich)	Screen printed graphite electrode modified with Prussian Blue (0.07 cm ²)	Drop casting of 5uL of mix: 25 uL of AOX solution, 4% BSA, 8 uL of 5% Nafion and 5 uL of 2.5% GA solution	-	0.05 – 0.5	-
2010 [35]	Pichia Pastoris (Sigma-Aldrich)	Pt electrode (0.12 cm ²)	Electrodeposition of the enzyme in three different conductive polymers' matrices (PPY, PEDOT, PEDOP)	21.4 uA/(M*cm2) (Ppy, PEDOP) 22.2 uA/(M*cm2) (PEDOT)	0 – 1750	170
2008 [22]	Hansenula sp. (Sigma-Aldrich)	Carbon film electrodes modified with poly(neutral red) PNR (0.2 cm ²)	Drop casting 10 uL of mixture composed of 10 uL of enzyme solution (AOX+BSA) mixed with 5 uL of GA solution (2.5%)	171.8 nA/mM	0 – 0.7	0.029
1996 [28]	«Hansenula Polymorpha (Sigma-Aldrich) «Hansenula Polymorpha stabilised with Dextrane (Leeds Biochemical) «Candida Boidinii (Genzyme) «Pichia Pastoris (Sigma-Aldrich)	Carbon paste electrode (0.049 cm ²)	For every AOX species, 4 electrode types were prepared by mixing graphite powder with enzyme solution: I) AOX+HRP II) AOX+HRP + LA III) AOX+HRP + PEI (covalent coupling for AOX CB) IV) AOX+HRP-Os (hydrogel made with PVI-Os) Best results: <u>CB-HRP-PEI</u> , <u>PP-HRP-Os</u>	0.351 uA/mM 1.31 uA/mM (CB-HRP-PEI -- a, PP-HRP-Os -- b)	0.25 – 2 0 – 4	0.015 0.010
2006 [32]	Pichia Pastoris (Sigma-Aldrich)	Au electrode (0.12 cm ²)	Three sensors prepared: I) pyrrole and AOX solution form a PPY-AOX film II) overoxidized PPY film + drop casting of 2uL enzyme solution (10uL AOX, 30uL 2.5% GA, 8mg BSA) III) pOPD film + drop casting of	282.8 nA/mM (PPY _{ox} /BSA-GA)	0.01 – 0.75	0.0023

			2uL enzyme solution (10uL AOX, 30uL 2.5% GA, 8mg BSA)			
2015 [34]	Pichia Pastoris (Sigma-Aldrich)	Glassy carbon electrode (0.196 cm ²)	Au nanoparticles stabilized with AOX, encapsulated with PANI Chitosan and Nafion to cover the dispersed np on the electrode	68.3 uA/(mM*cm ²)	0.01 – 4.7	0.007
2021 [24]	Pichia Pastoris (Sigma-Aldrich)	Screen printed carbon electrodes modified with PANI (0.11 cm ²)	Drop casting of 5uL 2.5% Nafion, 40uL 0.1% GA and 40uL AOX solution	1.705 uA/(mM/L)	0.01 – 1	0.045
2018 [36]	Pichia Pastoris (Sigma-Aldrich)	Pt electrodes	Electrodeposition of calcium alginate hydrogel to immobilize the enzymes AOX, HRP	-54 nA/(g/L)	0 – 21,7	-
2007 [39]	Hansenula sp. (Sigma-Aldrich)	O ₂ sensor (Pt cathode and Ag/AgCl anode) (2 mm diameter)	Drop casting of AOX solution mixed with chitosan onto an eggshell membrane	3.02 mg/(mM*L) (O ₂ sensor)	0.06 – 0.8	0.03
2003 [26]	Pichia Pastoris (Sigma-Aldrich)	pellets: 3 mm diameter	Mix of 0.28g graphite, 200uL AOX, 11mg HRP, 0.4mL PBS, ferrocene and Teflon	55.1 uA/mM	0.02 – 2	0.005

2.3 Non-enzymatic ethanol sensors

The topic of non-enzymatic ethanol sensors has not been investigated deeply, as the gold standard has always been to work with enzymes thanks to their great selectivity. On the other hand, the energy field has been focusing, over the last decades, on sustainable energy and the devices used for this purpose. In particular fuel cells are of great interest in this field and many fuels have been studied for this purpose, in between which ethanol results as non-toxic and easy to store. Therefore, the ethanol oxidation on non-enzymatic catalysts has been investigated deeply in this industry type [40]. Multiple materials have been studied for this purpose, such as platinum, palladium, nickel and gold. In the next sections the focus will be on platinum as the material for non-enzymatic ethanol sensing.

2.3.1 Ethanol oxidation reaction on platinum

The ethanol oxidation reaction (EOR) on the surface of Pt catalyst can follow two different pathways, as shown in Figure 2.6 [40]:

- I. C1 pathway: the so-called complete oxidation, which consists in the oxidation of ethanol into carbon dioxide freeing a total of twelve electrons.
- II. C2 pathway: the so-called partial oxidation, which consists in the oxidation of ethanol into acetaldehyde or acetic acid, freeing respectively two and four electrons.

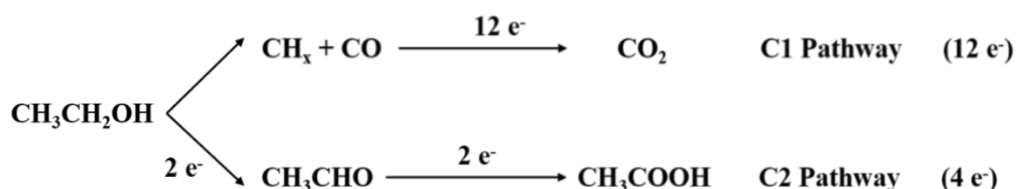


Figure 2.6: EOR mechanisms on Pt catalyst. Figure adapted from [40]

In the C1 pathway the C-C bond is cleaved, giving rise to intermediate compounds such as CH_x , which are then oxidised into CO, that is further oxidised into CO_2 [40].

The EOR mechanism has been investigated to determine the reaction intermediates and the conditions that favour the two pathways. The ethanol oxidation on Pt depends on the composition and pH of the electrolyte, the voltage at which the reaction occurs, the temperature, the crystallographic orientation of the catalyst and the ethanol concentration [40].

2.3.2 Influencing factors on EOR

Many parameters influence which EOR pathway occurs when ethanol is present in solution. The main ones are ethanol concentration, pH and composition of the electrolyte in which the analysis is conducted, the applied potential to the electrode, and the crystallographic orientation.

A study on polycrystalline Pt in an acidic environment showed that if **ethanol concentration** is lower than 0.1M, the C1 pathway is favoured. More specifically, for ethanol concentration equal to 25mM there is a peak of production of CO₂. Instead, when ethanol concentration is higher than 0.1M, specifically from 0.2M up, the main product of the EOR is acetaldehyde. This can be explained by the fact that when the analyte concentration is very high, the catalyst's sites are not able to adsorb water and cause its dissociation into H⁺ and OH⁻. This latter step is, in fact, crucial for the oxidation of acetaldehyde into acetic acid and of adsorbed CO groups into CO₂, therefore the rate of ethanol oxidation is low at high ethanol concentrations [41]. Figure 2.7 shows the influence of ethanol concentration on the EOR as well as the oxidation reaction of adsorbed CO that takes place on the surface of the electrode, thanks to the presence of adsorbed dissociated water molecules.

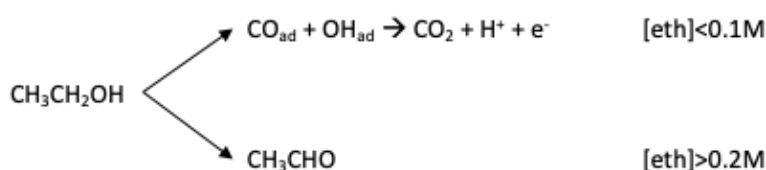


Figure 2.7: Scheme of ethanol concentration influence on the EOR

Another important parameter that influences the EOR mechanism is the **electrolyte**. In a study conducted in 2010, a polycrystalline Pt electrode was tested in different solutions: perchloric acid (0.1M HClO₄), sodium hydroxide (0.1M NaOH) and phosphate buffer solutions (0.1M PBS) with pH varying from 2 to 12. The results showed that in alkaline media both C2 and C1 pathways take place and exhibit higher current densities than in acidic media. Moreover, the C1 pathway is promoted in the absence of strongly adsorbing anions, thus in perchloric acid and in sodium hydroxide. In the phosphate buffers instead, the anions get strongly adsorbed on the surface of the catalyst, therefore the C-C bond cleavage is hindered [42].

In the same study the influence of applied **potential** was also studied. It was noticed that at low applied potentials on a clean Pt surface, the production of CO/CO₂ and acetic acid is comparable. This can be explained by the fact that at low potentials the formation of oxidants, such as hydroxyl groups adsorbed on the surface, is low, therefore the oxidation of the adsorbed CH_x and CO into CO₂ as well as the oxidation of acetaldehyde into acetic acid, is limited. As the

potential increases, the oxidants' coverage of the catalyst's surface increases. At the same time, although, this higher coverage limits the adsorption of the analyte and therefore the cleavage of the C-C bond. For this reason, these two processes are always competing [42]. Therefore, as it was demonstrated in a study conducted in 2014 on Pt(111), the rate limiting step of the EOR is the adsorption of water and its dissociation. Thus, an ideal catalyst should adsorb intermediates weakly and water more strongly [43].

Finally, EOR is also strongly dependent on the **crystallographic orientation** of the catalyst. From a 2008 study the Pt(100) surface results as the best surface for the production of CO₂, while Pt(111) yields only products belonging to the C2 pathway. The selectivity towards the two pathways depends on how the atoms bind to the surface of the catalyst and the stability of hydroxyl groups adsorbed on the catalyst [44].

2.3.3 Additional elements influencing the EOR

To improve the catalytic activity of Pt and therefore increase the chances of completely oxidising ethanol into carbon dioxide, elements such as metals or oxides can be added to the catalyst [40]. If a metallic element is alloyed with platinum an **electronic effect** is yielded, which means that the valence electronic structure of the catalyst changes, resulting in a more reactive surface, able to bind adsorbed species more strongly [40]. Specifically, if Ru, Sn or SnO_x are added to the catalyst, a **bifunctional effect** results, which means that water dissociation is favoured on the surface of the catalyst [40]. This was demonstrated by a study which compared the ethanol catalytic performance of glassy carbon electrodes modified with only Pt (Pt/C), with Pt and SnO_x 8%weight (Pt/ SnO_x⁸/C) and with Pt and SnO_x 12% weight (Pt/ SnO_x¹²/C). The results show that as the quantity of SnO_x increases, the catalytic activity of the electrodes increases, yielding a higher transfer of electrons [45].

The two mentioned effects must be tuned to allow for a stronger binding of water over intermediates, but also to elicit the cleavage of the C-C bond. Many catalysts have, in fact, been realised by adding Sn or Ru to Pt, exploiting therefore only the bifunctional effect. These catalysts cause only the partial oxidation of ethanol into acetaldehyde or acetic acid, not yielding the maximum current. When an additional metal element is included in the catalyst, this promotes the cleavage of the C-C bond, resulting in the production of CO₂ and therefore the release of 12 electrons [40].

Many studies have compared the performance of differently modified electrodes in order to come to the previously mentioned conclusions. For example, in 2006 Pt-Ru/C and Pt-Ru-Ni/C electrodes were compared and it was shown that the

catalyst containing Ni had a better resistance to CO poisoning in acidic medium [46].

Six years later another study compared five electrodes in acidic medium: Pt/C, Pt-Sn/C, Pt-Re/C, Pt-Re-Sn/C %w(20:10:10) and Pt-Re-Sn/C %w(20:5:15) for ethanol sensing. The tri-metallic electrodes showed the better results, and the one with a lower percentage of Re has shown the best performance as it does not hinder the oxidation of intermediates [47].

Finally, in 2015 the performance of Pt, Pt-Rh, Pt-SnO₂, Pt-Rh-SnO₂ catalysts in acidic acid were compared and it was demonstrated that the tri-metallic catalyst yields the highest amount of CO₂ [48].

2.3.4 Nanostructuring of the electrodes

The addition of nanostructures on the electrodes has been used over the past decades in order to enhance the selectivity, sensitivity and LoD of electrochemical sensors. The nanostructuring of the electrodes does, in fact, increase the surface area yielding a better sensing performance in both enzymatic and non-enzymatic sensors [49]. It is possible to compute the enhanced area (electroactive surface area (ESA)) of the nanostructured electrodes from the CV curves of the electrodes.

Among other techniques used for the development of nanostructures, **electrodeposition** is a simple and effective method [50] as well as perfectly compatible with electrochemical sensors and very well adaptable to miniaturized electrodes [49]. This technique is carried out with the electrode to be nanostructured immersed in an electrolyte solution containing the metal salts of the metal that will constitute the nanostructures. The three-electrode setup is completed with a CE and a RE. The WE behaves as the cathode while the CE behaves as the anode. When a potential is applied between the WE and the RE, the metal ions in solution get reduced at the surface of the WE. Simultaneously, the CE gets oxidised creating new metal ions in solution [51].

This method has been used in multiple research studies with the aim of developing ethanol sensors [52], [53], [54], [55], [56], [57], as can be seen in Table 2.2. Usually, electrodeposition of Pt is obtained by applying different potentials to the electrode when in solution hexachloroplatinic acid (H₂PtCl₆) is present.

In a study conducted in 2015 the researchers investigated the influence of the metal salt concentration, of the applied potential and of the deposition time. The results showed that a higher concentration of H₂PtCl₆ yields a larger

electroactive surface area, whilst a higher applied potential promotes the formation of smaller nanostructures. The deposition time instead affects the shape of the nanostructures, causing them to be sharper as the time increases [50].

Multiple metals can be electrodeposited onto the WE by either exposing it to different electrolytes or by applying different potentials to yield the reduction of different ions [51]. For example, a trimetallic catalyst was obtained by electrodepositing Pt, Ru and Ni on a modified glassy carbon electrode (GCE), thanks to the application of pulsed potential in a solution containing salts of all three metals (0.2 M H₂SO₄, 1 mM H₂PtCl₆, 1 mM RuCl₃ and 1 mM NiSO₄) [55].

In other works, the electrode nanostructuration is based on other methods. For example, in 2011 nanoporous PtAg (NPS-Pt) and PtCu (NPC-Pt) were prepared by first dealloying Ag and Cu from Al using AgAl and CuAl foils respectively, and then by immersing these nanostructures into H₂PtCl₆ to let the galvanic replacement reaction between nanoporous metal structures and noble metal salts take place while stirring. These nanostructures were then mixed with carbon powder, ethanol and Nafion. The resulting ink was deposited onto a GCE [58]. Two years later the research group used the same protocol to deposit nanoporous PtCo and nanoporous PtNi onto two separate GCE [59], [60]. In another study in 2017, Pt nanoparticles were prepared with a water-in-oil method, and simply drop-cast onto a SPCE [61].

Table 2.2: List of non-enzymatic ethanol sensors, with focus on the electrodes used, the geometric area and the ESA, the nanostructuring technique, the analysis media and the sensing performance (sensitivity, LoD and linear range). In red are the catalytic elements.

Year of publication	Electrode	Electrode surface (cm ²)	Nanostructuring technique	Media	Electrochemical active surface area (computation method)	Sensitivity	Linear range (mM)	LoD (uM)
2015 [52]	ITO covered glass electrode	0.16	Pt and Ru nanoflowers were electrodeposited at -0.4V (vs Ag/AgCl) in 2mM H ₂ PtCl ₆ , 0.5mM RuCl ₃ and 0.2M H ₂ SO ₄	0.5M H ₂ SO ₄ 0.5M NaOH 0.1M PBS pH=7	1.11 cm ² (Cu upd stripping)	56,6 uA/(mM*cm ²)	0.025 – 9.5	5
2016 [53]	GCE modified with EGN-GO	0.03	Pt and Cu were electrodeposited at -0.2 V (vs SCE) in 1mM H ₂ PtCl ₆ , 100mM CuSO ₄ , 0.2M Na ₂ SO ₄ . Following CV in 0.5M H ₂ SO ₄ for porous structure	0.5 M H ₂ SO ₄	1.15 cm ² (H adsorption)	11000 mA/(mM*cm ²)	0.25 - 13	50
2017 [61]	screen printed carbon electrode	0.1256	drop casting of Pt nanoparticles dispersion prepared with water-in-oil method	1M KOH	4.56 cm ² (H adsorption)	12701 mA/mM	15 - 102	-
2019 [54]	Au electrode	0.0706	electrodeposition of Au nanoparticles at -3V (vs SCE) in 50mM HAuCl ₄ and 3M NH ₄ Cl. Following electrodeposition of Pt nanoparticles at -1V (vs SCE) in 4mM H ₂ PtCl ₆ , 0.1M KCl	0.5M H ₂ SO ₄	18.8 cm ² (H adsorption)	76 uA/(mM*cm ²)	0.05 - 43.3	2.3

2009 [55]	GCE coated with ionic liquid modified and MWCNT	0.07	Pt, Ru and Ni were electrodeposited by applying pulsed potential [-0.9;0]V (vs SCE) in 0.2M H ₂ SO ₄ , 1mM H ₂ PtCl ₆ , 1mM RuCl ₃ and 1mM NiSO ₄	0.5M H ₂ SO ₄	(potassium ferricyanide)	21 uA/(mM*cm ²)	0 - 38	50
2011 [58]	GCE	0.1256	nanoporous Ag (NPS) and nanoporous Cu (NPC) were added to H ₂ PtCl ₆ to create nanoporous PtAg (NPS-Pt) and nanoporous PtCu (NPC-Pt) respectively. These were then mixed with carbon, ethanol, Nafion and deposited onto the electrode	0.5M H ₂ SO ₄	(H desorption)	0.42 uA/(mM*cm ²) (NPS-Pt)	0 - 20 (NPS-Pt)	10 (NPS-Pt)
2013 [59]	GCE	0.1256	nanoporous PtCo mixed with carbon, ethanol, Nafion and deposited onto the electrode	0.5M H ₂ SO ₄	(H desorption)	0.53 uA/(mM*cm ²) (deduced from graph)	0 - 12	8
2013 [60]	GCE	0.1256	nanoporous PtNi mixed with carbon, ethanol, Nafion and deposited onto the electrode	0.5M H ₂ SO ₄	(H desorption)	0.43 uA/(mM*cm ²) (deduced from graph)	0.2 - 11	10
2013 [57]	Au electrode	-	electrodeposition of Pt nanoparticles in 7mM H ₂ PtCl ₆ solution. Fe ₃ O ₄ MNPs were drop casted onto the electrode	0.1M H ₂ SO ₄ - Na ₂ SO ₄ pH=2	-	420 uA/(mM*cm ²)	0.02 - 0.11	3.2

State of the art for ethanol sensors

2019 [56]	MoS ₂ modified ITO electrode	-	electrodeposition of Pt by applying -0.2V (vs SCE) in 2mM H ₂ PtCl ₆ and 0.1M H ₂ SO ₄	0.1M H ₂ SO ₄	(H desorption)	-	-	10 ⁵ (only test made)
-----------	---	---	--	-------------------------------------	----------------	---	---	----------------------------------

2.4 Conclusion

In conclusion, amperometric ethanol sensors based on enzymes are primarily developed using AOX and operate by sensing the increase of hydrogen peroxide concentration. To lower the applied potential to the electrode needed to obtain the oxidation of H_2O_2 , electrocatalysts, mediators and additional enzymes are employed. Moreover, immobilization methods by using membranes, crosslinkers, and covalent binding, enhance enzyme loading and help retain the activity of these proteins. However, the main limitations of enzymatic sensors include the short lifetime of enzymes, the influence of environmental factors on the enzyme activity, and the low efficiency of the electron transport between the bioreceptor and the electrode.

Non-enzymatic ethanol sensors based on Pt provide a viable alternative to enzymatic sensors. They are less sensitive to the environment and exhibit more direct and efficient electron transfer. The main techniques that can be used to improve the sensor's performance are nanostructuring of the electrode as well as the inclusion of additional elements. The primary drawback of non-enzymatic sensors is the lack of specificity to the target analyte, which can lead to erroneous sensing of interferents, and the adsorption of reaction intermediates and byproducts on the electrode surface.

Chapter 3: Experimental work: Enzymatic sensor

This chapter describes the fabrication choices and methods used to develop the enzymatic sensor, moreover it reports the performance evaluation of these sensors when applied to a neutral solution containing the target analyte. In fact, the alcohol oxidase best working pH is between 7.5 and 8.5 based on the yeast it is derived from [62].

3.1 Electrode modification

The enzymatic sensor was prepared following the protocol established by Rusli in 2021 for the development of sensors capable of detecting glucose and lactate during the beer fermentation process [63]. To simplify the manufacturing process and enhance reproducibility, no mediators, electrocatalysts, or additional enzymes were incorporated in the sensor's fabrication. The protocol involved immobilizing the enzyme by crosslinking it with BSA using GA [63]. This immobilization technique is widely used in enzymatic ethanol sensors, as highlighted in Table 2.1.

The enzymatic sensors developed in this project are based on the enzyme alcohol oxidase (AOX). AOX can be derived from three **yeast species**: *Pichia pastoris*, *Candida boidinii* and *Hansenula polymorpha*. For this study, the enzymes derived from the latter two species were selected because they are available in powder form. Lyophilized powder enzymes generally exhibit superior storage stability compared to enzymes purchased in solution, provided they are stored under appropriate conditions [64].

3.1.1 Materials and methods

For the development of *Hansenula* AOX-based electrodes, the lyophilized enzyme was purchased from Creative Biogene, in a quantity of one KU. One unit of enzyme is defined as “the amount of enzyme that generates 1 umole of

H₂O₂ from methanol per minute at pH 7.5 at 25°C" [65]. The enzyme's specific activity is reported as 10-40 units/mg, with the quality control test resulting in 13.1 units/mg.

The *Candida Boidinii* AOX was purchased in powder form from Sigma Aldrich in a quantity of 50 units, with specific activity of 5-15 units/mg.

All electrochemical measurements were conducted at room temperature using a potentiostat (Autolab PGSTAT302N). The electrodes used to develop the sensors were disposable Metrohm DropSens Pt SPEs featuring a 4mm diameter Pt WE, a Pt CE and a Ag/AgCl RE. The experiments on the *Hansenula* based electrodes were conducted using the internal RE and CE from the screen-printed electrode setup with a compatible connector purchased from Metrohm DropSens. An external commercial double-junction Ag/AgCl RE and a platinum wire CE were used to conduct the experiments on the sensors that included the *Candida Boidinii* AOX.

The experiments used a 100 mL of 0.1M PBS (pH 7.4) obtained from VWR. The ethanol stock solution was prepared by diluting ethanol absolute purchased from VWR with the PBS.

Cyclic voltammetry tests were conducted between -1 V and 1 V, with a scan rate of 100 mV/s, until the voltammograms were overlapping.

Chronoamperometry studies were conducted with magnetic stirring at 300 rpm. A potential of 0.7 V relative to the RE was applied to ensure the oxidation of H₂O₂ produced during the enzymatic oxidation of ethanol. The CA tests were conducted for ethanol concentrations ranging from 0 to 20 mM. Each measurement was repeated with three electrodes to ensure reproducibility.

3.1.2 Immobilization protocol

The enzymatic electrode preparation relies on the usage of the drop casting technique, where a small volume of enzyme is deposited on the WE surface.

The following is the protocol used for a glucose sensor based on the enzyme glucose oxidase:

- I. In a first phase, 3 mg of BSA were dissolved in 93.8 uL of PBS, then 1.2 uL of GA were added to the solution and lastly 2 mg of glucose oxidase (GOX) were mixed in.
- II. A volume of 0.1 uL of this solution was deposited on the surface of the electrode and left to dry for 60 minutes.

III. The electrodes are left to dry in the freezer for 24 hours before being ready to be used.

This protocol was developed for a 0.26 mm² WE and the enzyme used had an activity of 100-250 units/mg, resulting in an enzyme loading of 0.8097-2,024 units/mm² [63].

For this study, adjustments were made to account for the larger area of the WE, which is 12.566 mm². Based on a study reported in 2012, the drop-casting volume suited for this area is 10 uL corresponding to 0.119 units/mm² [23].

Two batches of sensors were prepared for both enzyme species. While the PBS, GA and BSA quantities remained consistent with the original protocol, the enzyme loading is different.

Regarding the electrodes that include *Hansenula*, the first batch was prepared by mixing 2 mg of AOX in the solution to drop cast, which resulted in a loading of 0.2186 units/mm². The other set, instead, was characterized by a loading of 1 unit/mm² and was achieved by including 9 mg of AOX in the solution to drop cast.

The two sets of electrodes that included *Candida* AOX, were prepared by using 2 mg and 19.8 mg of enzyme, to obtain a loading of around 0.0835-0.251 units/mm² and 0.829- 2.488 units/mm², respectively.

3.2 Performance evaluation

The immobilization procedure used for electrode functionalization proved to be inefficient. After every CV and CA test, the enzyme layer flaked off. Additionally, the enzyme solution prepared by including the highest mass of the enzyme (9mg for *Hansenula*, 19,8mg for *Candida*) were highly viscous, making them difficult to pipette and resulting in uneven coverage on the WE surface as shown in Figure 3.1.

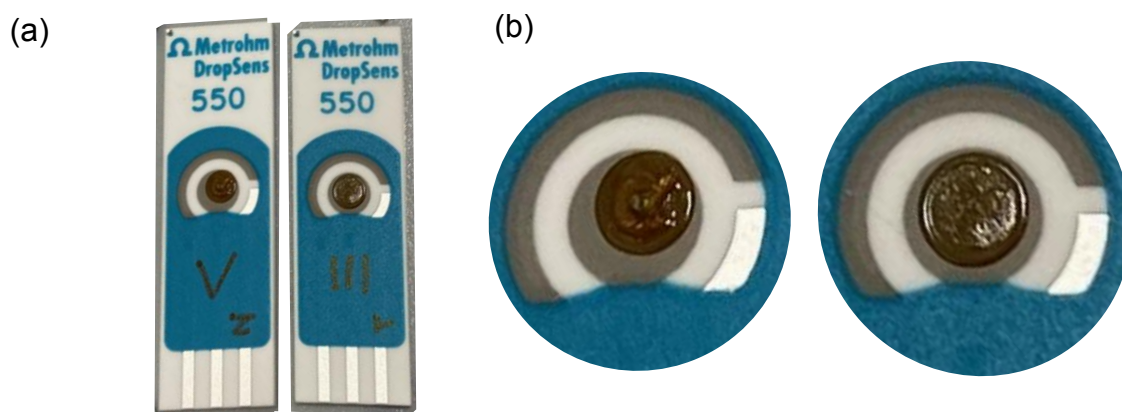


Figure 3.1: Photos of the modified SPE with the enzyme *Hansenula*. In a) and b) the electrode on the left is prepared by including 9mg of enzyme, the one on the right 2mg. a) 24 hours after the deposition; b) Zoomed-in view of the sensing area.

All the CA tests of the modified electrodes showed no response to ethanol, as shown in Figure 3.2.

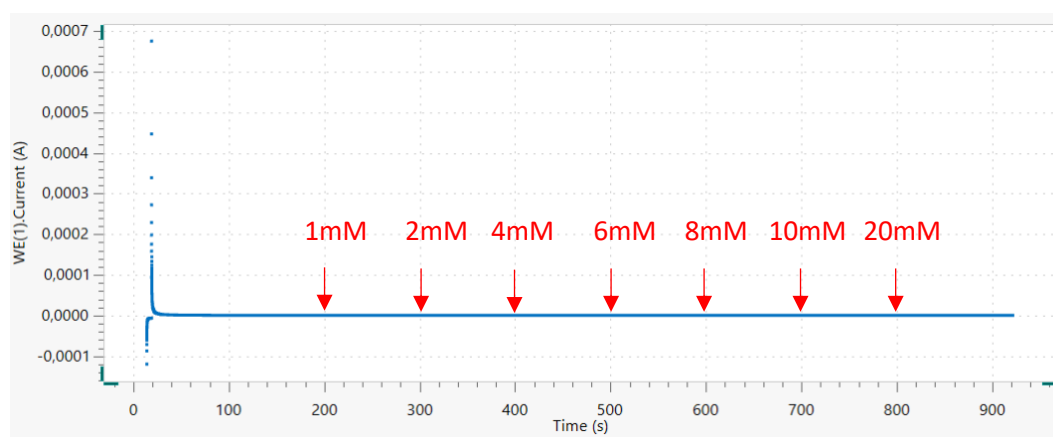


Figure 3.2: CA response of *Hansenula* electrodes in 0.1 M PBS with consecutive ethanol spike. Stirring rate: 300 rpm; applied potential: 0.7 V vs Ag/AgCl RE

Due to the poor stability of the enzyme layer and the high cost of the enzymes, further efforts to develop enzymatic ethanol sensors were not pursued.

3.3 Summary and contributions

This chapter describes the development of enzymatic ethanol sensors. The main topics are the choice of the AOX-producing yeast species, the immobilization protocol and the performance evaluation for the detection of

ethanol. The key contribution of this chapter is the adaptation of previously developed protocol to include the enzyme AOX on SPEs.

Given the high cost of enzymes and the results with established enzyme immobilization protocols/units of enzyme per area, the focus of this thesis shifted to non-enzymatic ethanol sensing solutions, which are described in the next chapter.

Chapter 4: Electrode nanostructuring and pre-screening

This chapter describes the methods used for electrode nanostructuring and the evaluation of the performance of the sensors in the presence of ethanol in acidic, neutral and alkaline environments.

There are two primary approaches to enhance the performance of non-enzymatic sensors: the addition of a metal to promote the formation of alloys, or the nanostructuring of the electrode surface. As explained in Section 2.3.3, alloying Pt with other elements improves the chances of obtaining CO₂ from EOR, thus yielding a higher current. In Section 2.3.4, it was explained how nanostructuring of electrodes causes an increase of the ESA, yielding an increase of the surface on which ethanol is oxidised.

In this thesis, the nanostructuring of electrodes was conducted using two electrodeposition techniques. These were compared in terms of enhancement of the electrochemical active surface area (ESA) and of catalytic performance in the presence of the target analyte.

4.1 Materials and methods

Nanostructuring of electrodes was achieved using two electrodeposition techniques. In both methods, platinum was electrodeposited from an aqueous solution containing 25 mM H₂PtCl₆ and 50 mM H₂SO₄ [49], [63]. In particular, the first technique, LSV, is based on the application of a potential that varies linearly in time at a certain scan rate, while the second method, CC, is based on the application of a constant potential. In the latter protocol the solution is stirred at 500 rpm using magnetic stirrers.

The first method is called LSV electrodeposition. It was implemented in a study in 2019 to deposit Pt nanostructures onto gold microelectrodes [49]. The LSV was conducted at a scan rate of 100 mV/s using two different potential ranges: between 0 and -0.6 V or between 0 and -0.8 V relative to Ag/AgCl RE. In the same study, it was demonstrated that the latter potential range was more effective, therefore it was implemented in this project [49].

The second method used is called chronocoulometry (CC) and it was used in a study in 2021 to deposit Pt nanostructures onto Pt electrodes [63]. The deposition of nanostructures is done by applying a constant potential over a period in order to control the charge passing through the electrode. In the original protocol the potential applied was -0.06 V towards Ag/AgCl RE in order to deposit a 25 mC charge on a 0.7854 mm² electrode. For this study, the charge was scaled proportionally to account for electrodes with a surface area around 16 times larger, yielding a charge of 400 mC [63].

In both procedures, the electrodes were first cleaned with CV in nitrogen purged 0.5 M H₂SO₄ until overlapping cycles were observed. The potential range used was between -0.2 and 1 V, with a scan rate of 100 mV/s. After cleaning, electrodes were rinsed with deionized (DI) water, dried with N₂, and subjected to electrodeposition. Post-deposition, electrodes were again rinsed, dried, and underwent a material activation *via* CV test under identical conditions to assess the surface area enhancement.

The LSV electrodeposition was carried out using an Autolab potentiostat, while the CC technique was executed using the Gamry 600+ potentiostat. In both procedures the RE is an external double junction Ag/AgCl electrode while the counter electrode is a Pt mesh. The working electrodes used are Pt SPE purchased from Metrohm DropSens with a 4 mm diameter WE (area 12.56 mm²). Experiments were conducted in triplicates.

There are mainly two techniques to evaluate the electroactive surface area of electrochemical sensors. The first one is by computing the area underneath the CV acquired in H₂SO₄ solution and related to the Pt oxide formation and subsequently dividing it by a factor of 420 uC/cm², related to a 1 cm² atomically smooth Pt electrode [50]. The second one consists in the computation of the area underneath the CV acquired in H₂SO₄ solution and related to the hydrogen adsorption/desorption peak and subsequently dividing it by a factor of 210 uC/cm², which is the charge associated with the H deposition [53]. In this work the first method is used.

The roughness factor (Rf) is a measure of the roughness of a surface. The higher this factor is, the higher is the nanostructuring. The Rf and the ESA are, in fact, proportional quantities.

The computation of the roughness factor and ESA was obtained using the following steps:

- I. Computation of the area of the peak related to the Pt oxide formation underneath the CV acquired in H_2SO_4 solution. The potential range for the computation of this area was defined to be between 0.2 V and 0.8 V.
- II. Subtraction of the electrochemical double layer current density. This parameter is defined as the product between the potential range related to the Pt oxide formation and the current corresponding to the lower limit of this potential range. Figure 4.1 shows a visual representation.
- III. Division by the scan rate, to obtain the charge deposited.
- IV. Division by the conversion factor $420\mu\text{C}/\text{cm}^2$, to obtain the ESA.
- V. Division by the area of the electrode, to obtain the roughness factor.

These computations were done in MATLAB, in particular, in order to compute the area underneath the CV, the MATLAB function *trapz* was used.

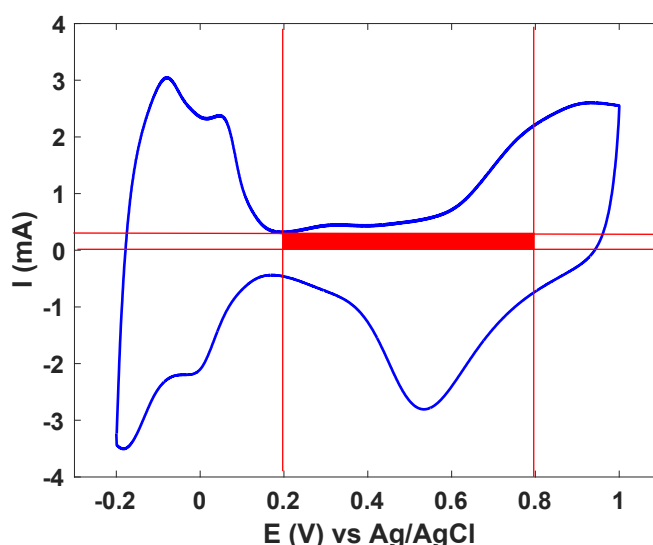


Figure 4.1: Representation of a CV scan in H_2SO_4 after nanostructuring. The red rectangle represents the electrochemical double layer current density.

Finally, CV measurements were conducted in order to evaluate the performance of the electrodes for sensing ethanol. They were performed using an Autolab potentiostat, double junction Ag/AgCl external RE and a Pt wire CE. They were conducted in all environments: acidic (0.5 M H_2SO_4), neutral (0.1 M PBS, pH 7) and alkaline (1 M KOH). In particular, the PBS was prepared using monosodium phosphate (NaH_2PO_4) and disodium phosphate (Na_2HPO_4) in order to avoid the presence of chlorides that can poison the surface of the catalyst. The tests in chloride-free PBS were conducted in triplicates. The scan rate used for these

tests was 100mV/s and the potential range was between -0.2 and 1 V. For ethanol additions, the stock solution was prepared by diluting ethanol absolute with the chloride-free PBS.

4.2 Characterization of the nanostructured electrodes

To compare the results of the two nanostructuring techniques, a morphological characterization was performed using a scanning electron microscope (SEM). Additionally, the ESA and the Rf were computed.

4.2.1 Morphological characterization

SEM images reveal that the nanostructuring obtained with the CC technique is much higher and more defined compared to the LSV results. The nanostructures are, in fact, bigger, therefore more visible and recognisable in the SEM image of the electrodes modified with the LSV deposition technique. These observations are evident in Figure 4.2.

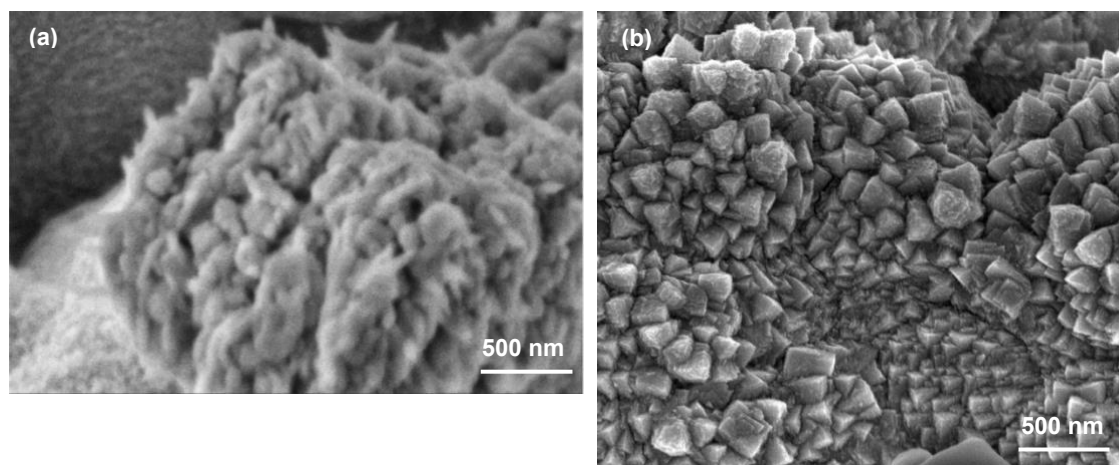


Figure 4.2: SEM images of the nanostructured electrodes. a) Result of CC electrodeposition, b) Result of LSV electrodeposition.

4.2.2 Evaluation of electroactive area and roughness factor

To evaluate the increase of the catalytic activity of the nanostructured electrodes, CV tests were conducted in sulfuric acid before and after electrodeposition, as shown in Figure 4.3:

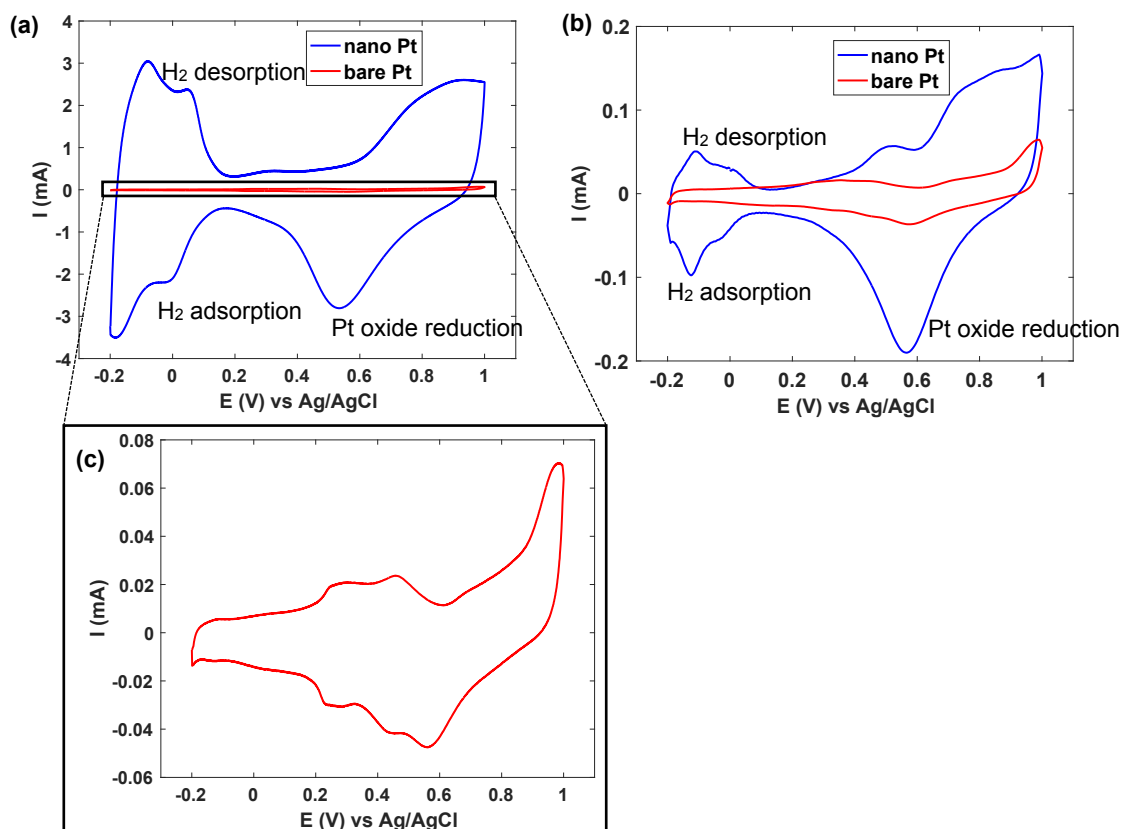


Figure 4.3: Comparison of CV scans in 0.5 M H_2SO_4 before and after electrodeposition. a) CV scan of CC nanostructured electrodes (blue) and bare Pt electrodes (red), b) CV scan of LSV nanostructured electrodes (blue) and bare Pt electrodes (red), c) Zoom in of CV scan of bare Pt electrodes. Scan rate: 100 mV/s.

As can be noticed in Figure 4.3 (a) and (b), two peaks, both cathodic and anodic, between -0.2 V and 0.1 V represent the H₂ adsorption/desorption. The cathodic peak around 0.5 V, instead, refers to the reduction of the Pt oxide formed during the positive scan. In the bare Pt scan (Figure 4.3 (c)) no significant peaks can be observed. Notice the different order of magnitude of the output current between the CV scans of the nanostructured electrodes and the CV conducted with the bare Pt electrodes.

The magnitude of the output current of the CV conducted after the LSV deposition technique is around 10 times smaller than the one recorded after the CC deposition (Figure 4.3 (a), (b)). Therefore, it can be concluded that the CC nanostructuring is more effective than the LSV method.

The computation of the ESA and of the roughness factor quantitatively represents this different nanostructuring efficiency. As shown in Table 4.1, the ESA, and the Rf for electrodes modified with the CC technique are approximately 15 times higher than those modified with the LSV technique. This

difference can be attributed to the fact that a 16 times higher charge passes through the electrode in the CC method in respect to the LSV method.

Procedure	ESA (cm²)	Rf	Applied charge (mC)
LSV	1,02 ± 0,02	8,07 ± 0,16	25,77 ± 0,76
CC	15,07 ± 0,02	119,89 ± 0,20	400

Table 4.1: Comparison between electrodeposition techniques in term of ESA, Rf and applied charge

In conclusion, the CC deposition technique outperforms the LSV technique. Therefore, the following experiments evaluating the sensor performance in the presence of the analyte were conducted solely with the CC-modified electrodes.

4.2.3 Performance evaluation

To evaluate the performance of the nanostructured electrodes, CV measurements were conducted to qualitatively calculate the sensitivity of the bare electrodes and the nanostructured electrodes in three different environments; neutral, acidic, and alkaline environments, both with and 0.5 M ethanol. The obtained results are shown in Figure 4.4.

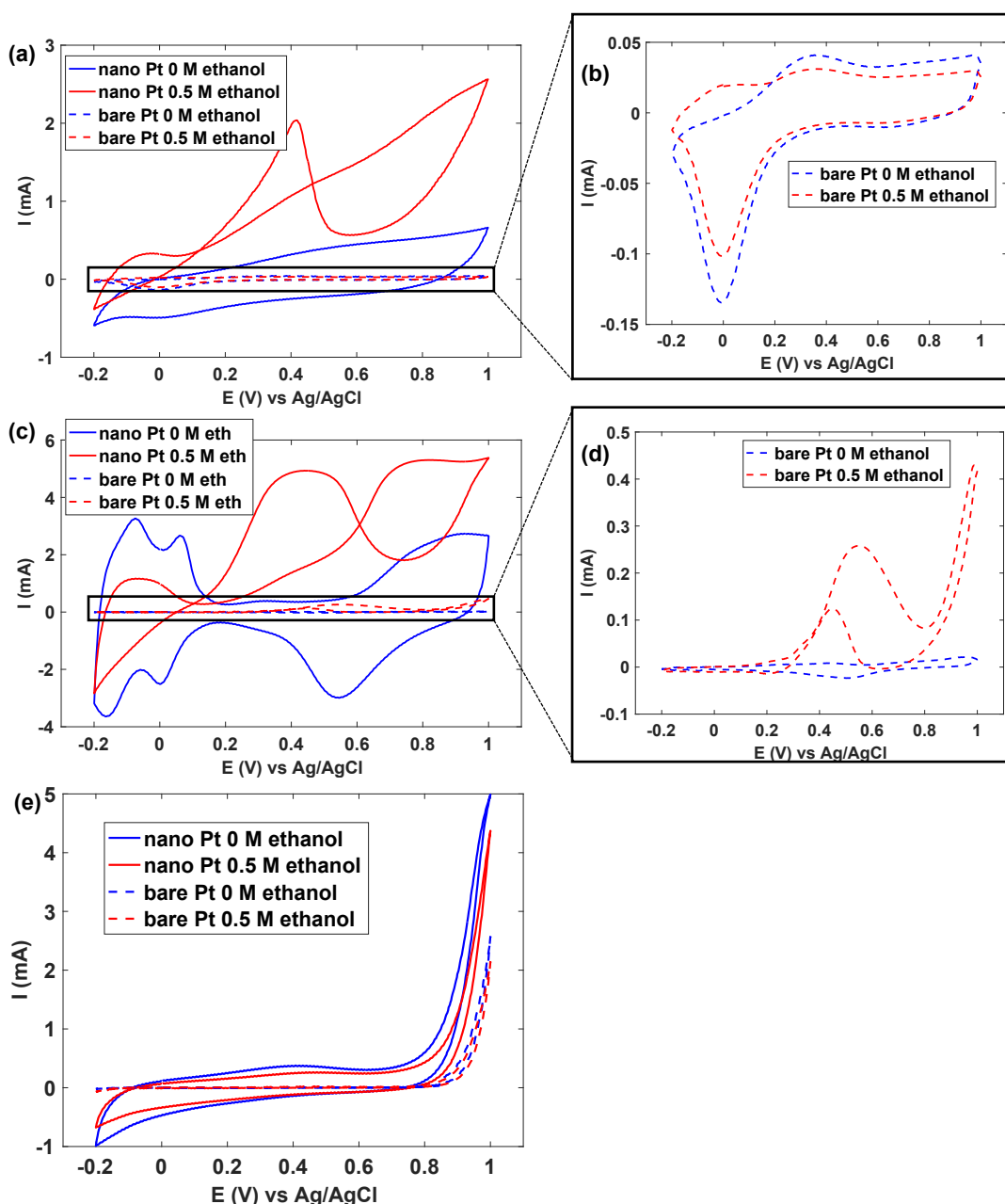


Figure 4.4: Comparison of bare SPE and nanostructured SPE in different environments in the absence and presence of 0.5 M of ethanol. (a) CV in 0.1 M chloride-free PBS (pH 7); (c) CV in 0.5 M H_2SO_4 ; (e) CV in 1 M KOH. (b), (d) Zoom ins of bare SPE in the neutral and acidic environment respectively. Sample size in (a), (b) $n = 3$. Scan rate: 100 mV/s.

As shown in Figure 4.4, the CV curves of bare SPEs in neutral (b) and alkaline (e) environments remain unchanged regardless of the presence of ethanol, indicating no ethanol sensing capability. In contrast, nanostructured SPEs exhibit distinct differences between blank scans and analyte scans in acidic and neutral environments (Figure 4.4 (a), (c)). When ethanol is added to the solution, the CV graphs show characteristic peaks, absent in the blank scan, corresponding to the oxidation and reduction of the analyte.

In the alkaline environment, no significant differences are observed between the blank and ethanol-containing solutions, suggesting that ethanol sensing is not feasible under these conditions (Figure 4.4 (e)). These findings indicate the potential for ethanol detection using nanostructured electrodes in acidic and neutral environments.

4.3 Summary and contributions

This chapter describes the nanostructuring of Pt electrodes using two different electrodeposition techniques and the pre-evaluation of the performance of the sensors for ethanol detection in solutions at different pH. The key contributions of this chapter include:

- I. Evaluation of the efficiency of two different analytical methods for nanostructuring electrodes and found in the literature, CC and LSV. ESA, Rf and applied charge were computed and compared. As a result of this comparison the CC method showed the best nanostructuring performance with a roughness factor of $119,9 \pm 0,2$.
- II. Assessment of the ethanol detection capabilities of the CC-modified electrodes in neutral, acidic, and alkaline environments. The findings show that the nanostructured electrodes exhibit a much better sensing capability in acidic and neutral environments, in respect to the bare electrodes.

In the next sections the focus will be the assessment of the analytical performance for sensing ethanol of the CC-modified electrodes in both neutral and acidic environments.

Chapter 5: Sensing of ethanol in neutral environment

In the previous chapter the pre-screening analysis showed that there is sensing of ethanol in neutral environment; therefore, in this chapter the nanostructured electrodes prepared using the procedure outlined in the previous chapter were tested in a neutral environment to investigate their performance in detecting ethanol.

5.1 Materials and methods

All the experiments were conducted at room temperature using an Autolab potentiostat, an external double junction Ag/AgCl RE, a Pt wire CE and the nanostructured electrodes as the WE. The volume of solution used was 50 mL.

The 0.1 M chloride-free PBS (pH 7) was prepared using monosodium phosphate (NaH_2PO_4) and disodium phosphate (Na_2HPO_4) to avoid the presence of chlorides, which could poison the catalyst surface. The ethanol stock solution was prepared by diluting absolute ethanol with the prepared chloride-free neutral PBS. Interferents stock solutions were prepared by dilution with chloride-free neutral PBS, kept in a refrigerator, and used within three days.

CV tests were conducted to determine the potential range and provide a qualitative measure of ethanol sensitivity. The scan rate was set to 25 mV/s.

CA tests were conducted to determine the potential at which the electrodes showed the highest response to ethanol. Moreover, CA tests were used to calculate the electrodes' sensitivity, establish the LoD, and evaluate the influence of interferents. In all experiments, the desired concentration of the analyte was spiked into the solution using micropipettes. Prior to the experiment, all electrodes were rinsed with DI water and dried. In these experiments the solution is stirred at 600 rpm using magnetic stirrers.

Before each CA test, the desired potential was applied for 120 seconds to allow the current to stabilize. After the stabilization, the current was recorded for different amounts of seconds based on the focus of the CA test.

For the CA tests conducted to determine the potential at which the electrodes showed the highest response to ethanol, a total of 150 seconds was recorded. The current averaged in the first 40 seconds represents the baseline current, while the current averaged in the last 80 seconds represents the electrodes' response to the analyte.

For the CA tests conducted to construct the calibration plot and the interference study, a total of 600 seconds and 700 seconds respectively was recorded. Additions of analytes were done every 100 seconds; therefore, the step current was computed averaging the current in the last 60 seconds.

The LoD can be computed using two methods: LoD intrasample and LoD intersample. In this Chapter only the latter has been computed as $3 \cdot \overline{Sb} / \bar{s}$, where \overline{Sb} is the standard deviation of the signals in the blank medium between all electrodes and \bar{s} is the average sensitivity. The error of this LoD coincides with the percentage standard error of the average sensitivity, which is the only influential error.

The computations were done with the Excel application.

5.2 Definition of the optimal potential window in CV

CV tests were conducted to identify the optimal potential window for the nanostructured electrodes in chloride-free neutral PBS with and without 2.5 mM ethanol. The upper potential was initially kept fixed at 1 V while the lower potential was decreased until the hydrogen evolution reaction (HER) peak became fully visible. The HER, which produces H₂ as a product of water electrolysis, typically defines the lower limit of CV curves. The best lower potential was determined to be -0.9 V, as can be observed in Figure 5.1:

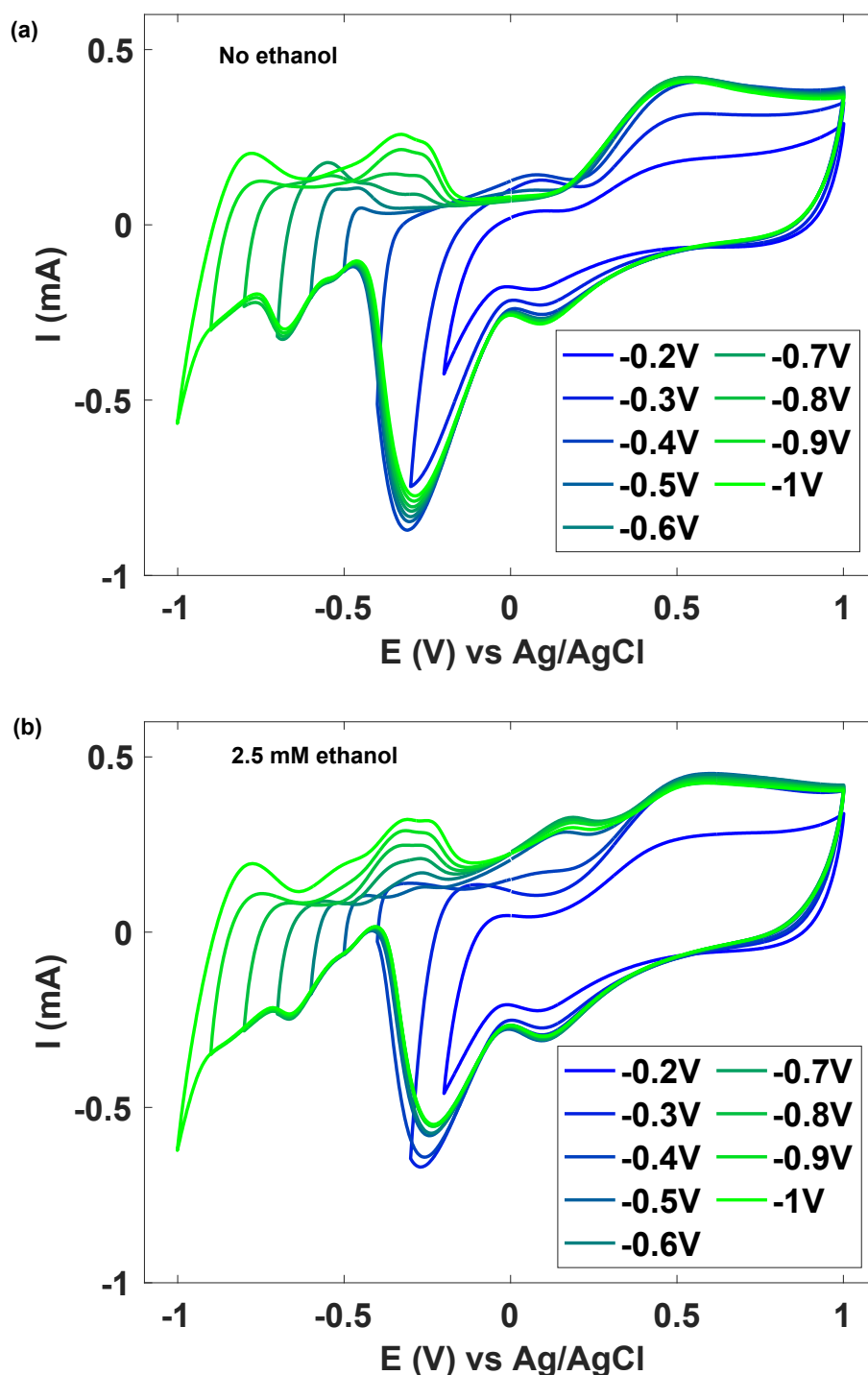


Figure 5.1: CV measurements to identify the lower potential of the window in 0.1 M chloride-free PBS (pH 7) without (a), and with 2.5 mM ethanol (b). Scan rate: 25 mV/s.

Next, the upper potential was evaluated by fixing the lower potential at -0.9 V and increasing the upper voltage potential until the oxygen evolution reaction (OER) peak was observed. The OER, which produces O_2 as a product of water electrolysis, marks the upper potential limit. The optimal upper potential was determined to be 1 V, as can be seen in Figure 5.2:

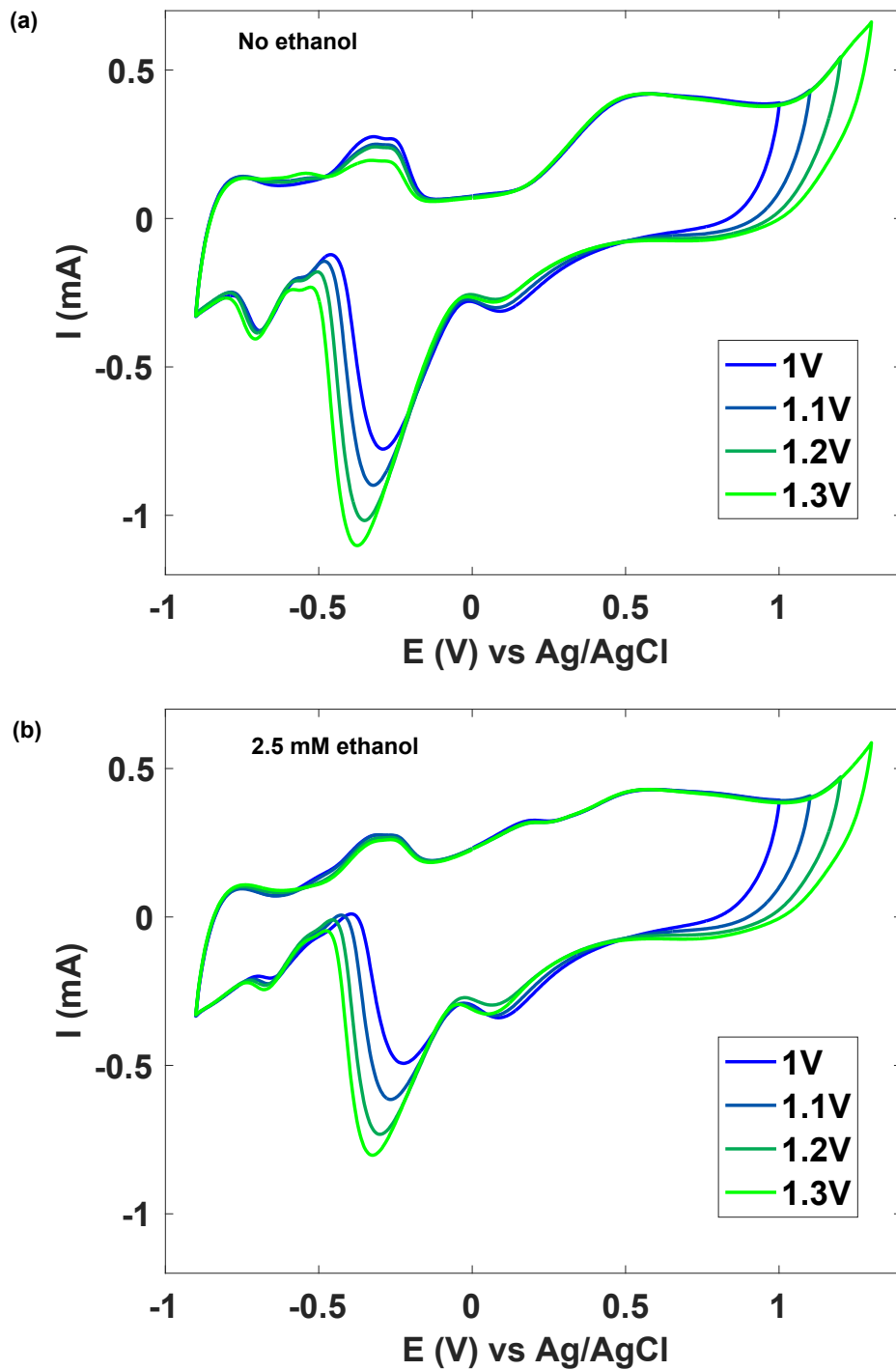


Figure 5.2: CV measurements to identify the upper potential of the window in 0.1 M chloride-free PBS (pH 7) without (a), and with 2.5 mM ethanol (b). Scan rate: 25 mV/s.

In conclusion, the optimal potential range for experiments in neutral environment was fixed between -0.9 and 1 V.

5.3 Identification of ethanol electrooxidation peaks in CV

After determining the CV potential window, the nanostructured electrodes were tested with different ethanol concentrations to assess the proportional increase of the output current relative to the analyte concentration.

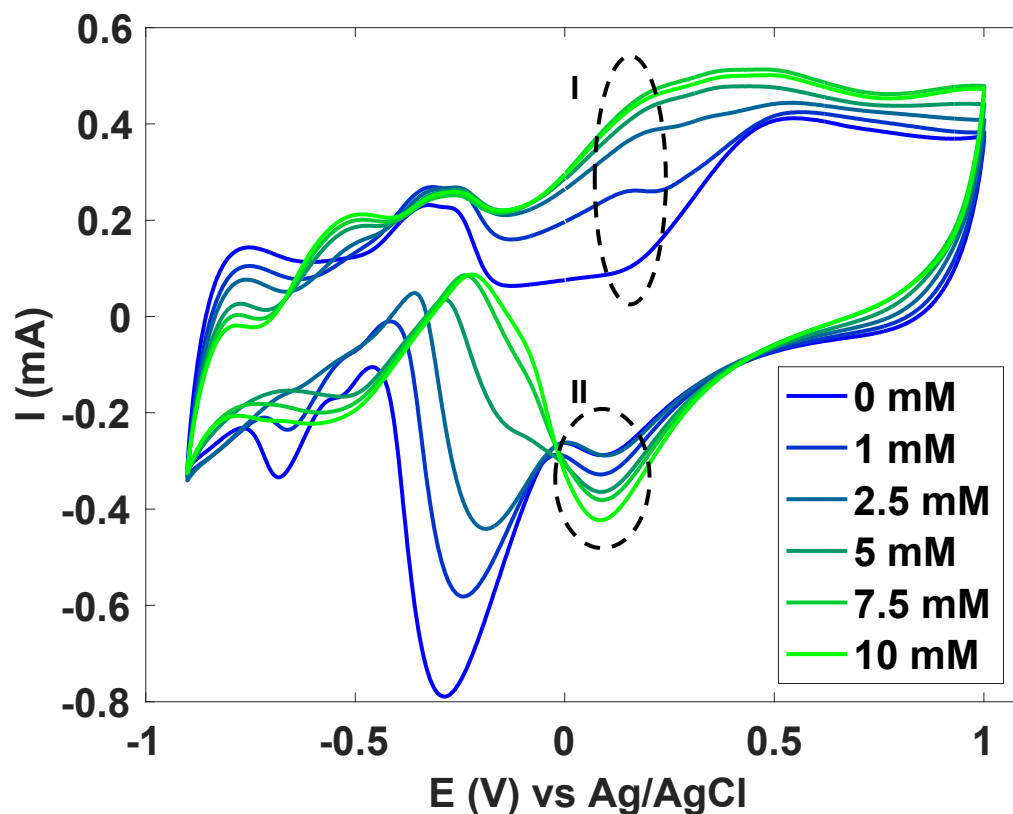


Figure 5.3: CV acquired for different concentrations of ethanol in the range 0-10 mM at nanostructured electrodes in 0.1 M chloride-free PBS (pH 7). Oxidation peak I) and reduction peak II) are more prominent as the ethanol concentration increases. Scan rate: 25 mV/s.

As shown in Figure 5.3, as the ethanol concentration increases there are multiple peaks appearing and increasing with the ethanol concentration increase. In particular, the blank scan showed no peaks in the positive potential range, while an oxidation peak appears in the presence of ethanol (peak I in Figure 5.3). Moreover, a reduction peak around 0.1 V becomes more pronounced with higher ethanol concentrations (peak II in Figure 5.3). Other peaks can be observed in the CV scan, but because of the complexity of the electrochemical reaction, it is not possible to determine which reaction is associated with each peak. Detailed analysis of the reactions occurring at the different potentials would require advanced techniques like *in situ* Fourier transform infrared spectroscopy (*in situ* FTIR) or differential electrochemical mass spectrometry (DEMS) [48].

5.3.1 Determination of the calibration potential in CA

CA was used to establish the potential yielding the highest ethanol response, with potentials ranging from 0 to 0.6 V. Figure 5.4 shows the step current as a function of the potential for three electrodes as well as the time-current plot.

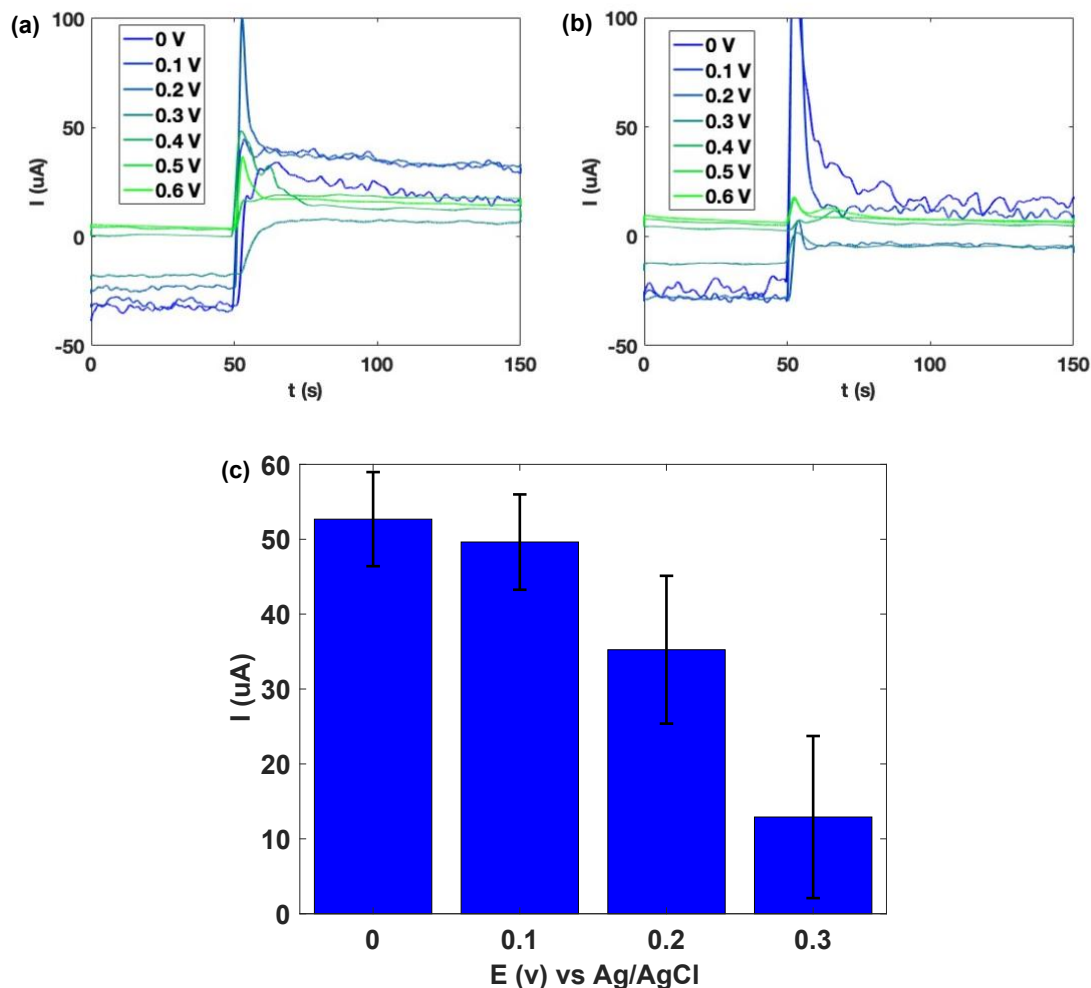


Figure 5.4: Time-current response to the addition of 2.5 mM ethanol at different applied potentials for electrode 1 (a), and 2 (b) in 0.1 M chloride-free PBS (pH 7). (c) CA average step current at different applied potentials; error bars: standard error of the step current for three electrodes. Sample size: $n=3$; stirring speed: 600 rpm.

As can be seen from Figure 5.4 (a) and (b), referring to the responses of two different sensors, there is some variability among the electrodes, which is due to possible fabrication differences. Considering that after 0.3 V only one sample was responding to ethanol, the step current – applied potential plot shows only the data for the potentials up to 0.3 V. The highest ethanol response was recorded at 0 V relative to Ag/AgCl RE, which was subsequently used for the calibration plot. The error on the average step current was computed as the standard error among the different electrodes, thus dividing the standard deviation of the step current measured for three electrodes by the square root of the number of electrodes.

5.3.2 Calibration in CA

CA was used to build the calibration plot by applying a working voltage of 0 V relative to Ag/AgCl RE. Figure 5.5 shows the time-current CA graph and the calibration curve.

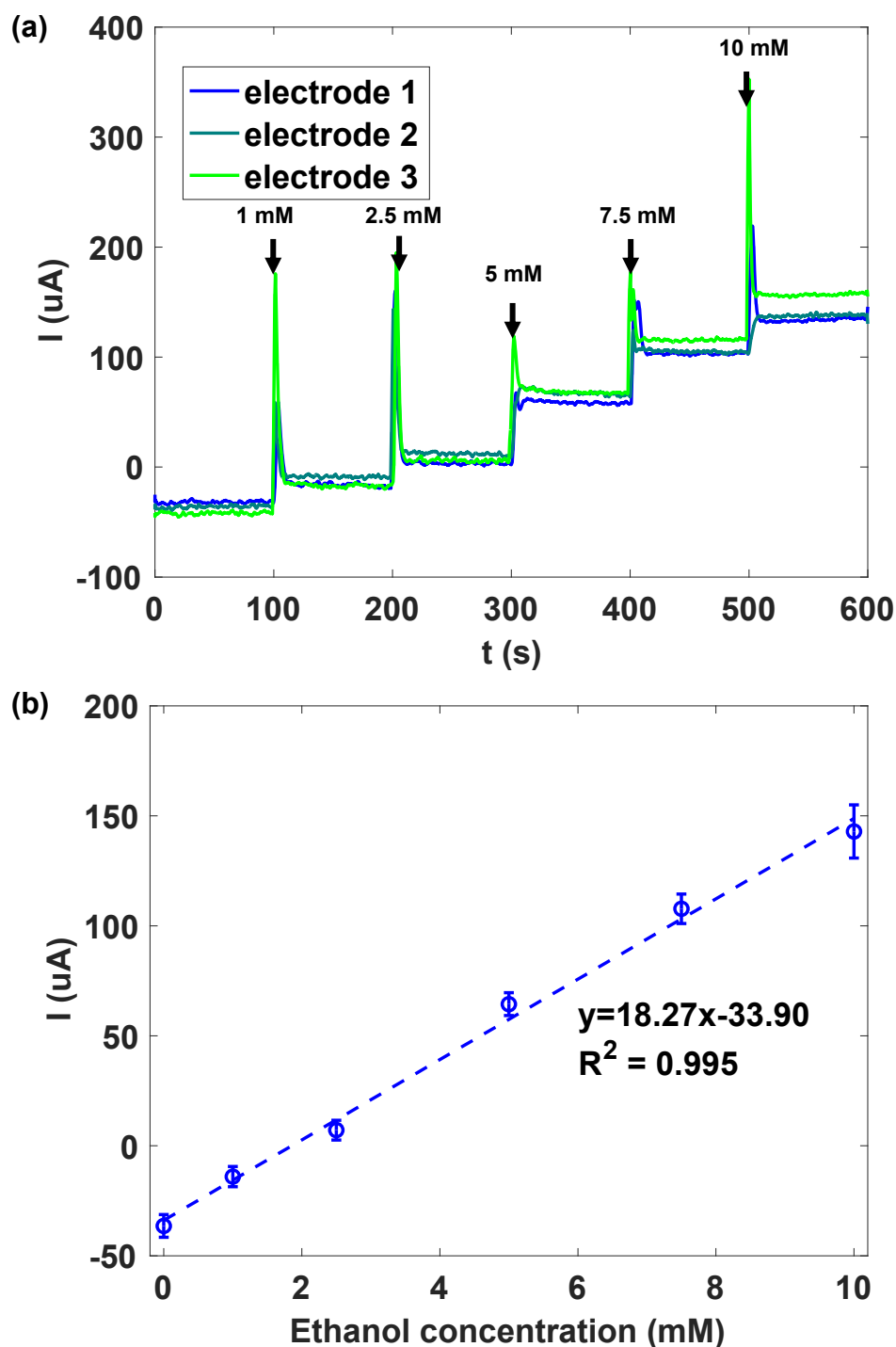


Figure 5.5: CA response to ethanol in 0.1 M chloride-free PBS (pH 7). (a) Time-current graph with ethanol additions every 100 s; (b) Average calibration curve; error bars: standard deviation

among three electrodes. Sample size: $n=3$; stirring speed: 600 rpm; applied potential: 0 V vs Ag/AgCl RE.

The average sensitivity obtained for three electrodes was 18.27 ± 0.93 $\mu\text{A}/\text{mM}$, and the mean sensitivity expressed per unit area is $145,46 \pm 7.42$ $\mu\text{A}/(\text{mM}\cdot\text{cm}^2)$. The error for the average sensitivity was computed as standard error, thus dividing the standard deviation of the sensitivity by the square root of the number of samples. The intersample LoD results to be 849 ± 43 μM , the error is equal to the percentage standard error of the sensitivity.

Considering the studies on non-enzymatic ethanol sensors presented in Table 2.2 (see Chapter 2), the sensors developed in this project demonstrate good sensitivity but more than a ten-time higher intersample LoD. This high discrepancy with literature could also be associated with the fact that intersample LoD value is always higher than intrasample LoD, therefore the reported studies might have computed the latter. Nevertheless, this study is innovative as it shows the feasibility of sensing ethanol in a neutral environment, which was shown before only by Hajian et al. [52].

5.4 Interference study

Understanding the effect of interferences is crucial in the development of a sensor, as one of its primary characteristics is selectivity. Among the interferents commonly tested for ethanol sensors in the literature, this study considered isopropanol, acetic acid, glucose, and ascorbic acid. Figure 5.6 shows the result of CA tests conducted to evaluate the effect of these interferents on ethanol sensing.

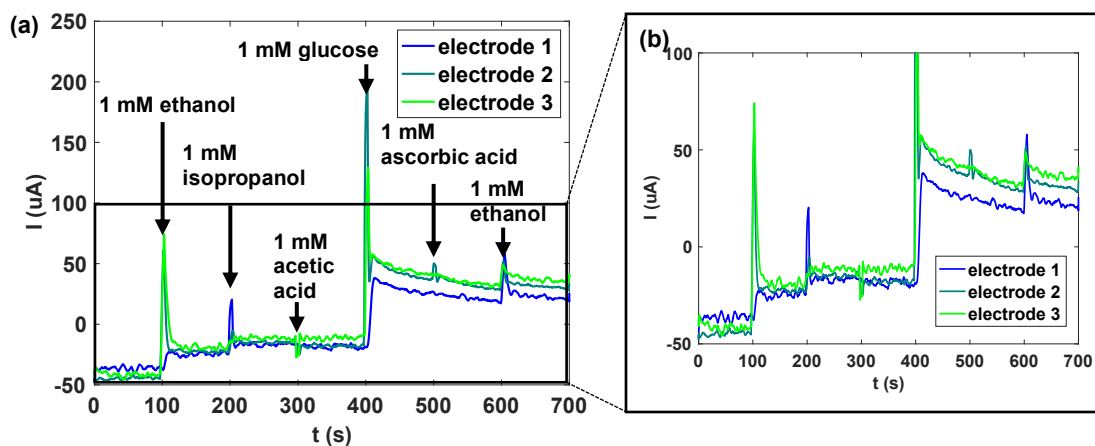


Figure 5.6: CA interference study in 0.1 M chloride-free PBS (pH 7). (a) Time-current plot with additions every 100 s; (b) Zoom in of (a). Sample size $n=3$; stirring speed: 600 rpm; applied potential: 0 V vs Ag/AgCl RE.

As can be seen from Figure 5.6, the influence of isopropanol, acetic acid, and ascorbic acid is negligible. However, the response of the electrodes to glucose is significantly higher than to ethanol. To better understand this cross-interference between ethanol and glucose, further experiments were conducted, as described in the next section.

5.4.1 Glucose cross-interference analysis

Alcoholic beverages typically contain both ethanol and glucose, making it essential to evaluate the cross-interference between these analytes.

In the past decades, non-enzymatic glucose sensors have been developed as an alternative to enzymatic sensors. Research on glucose sensors mainly focuses on monitoring blood glucose level for diabetes management. Among the materials that have been used to fabricate these sensors, platinum, as a noble metal, has shown high efficiency in glucose electrooxidation [7]. Notably, glucose oxidation into gluconolactone is favoured in alkaline and neutral pH due to the presence of reactive hydroxyl groups adsorbed on the catalyst surface [7]. In contrast, glucose reactivity was found to be lower in acidic media [66].

In this work, the influence of glucose on ethanol sensing was investigated by studying the sensitivity to ethanol in chloride-free neutral PBS with glucose (Figure 5.7).

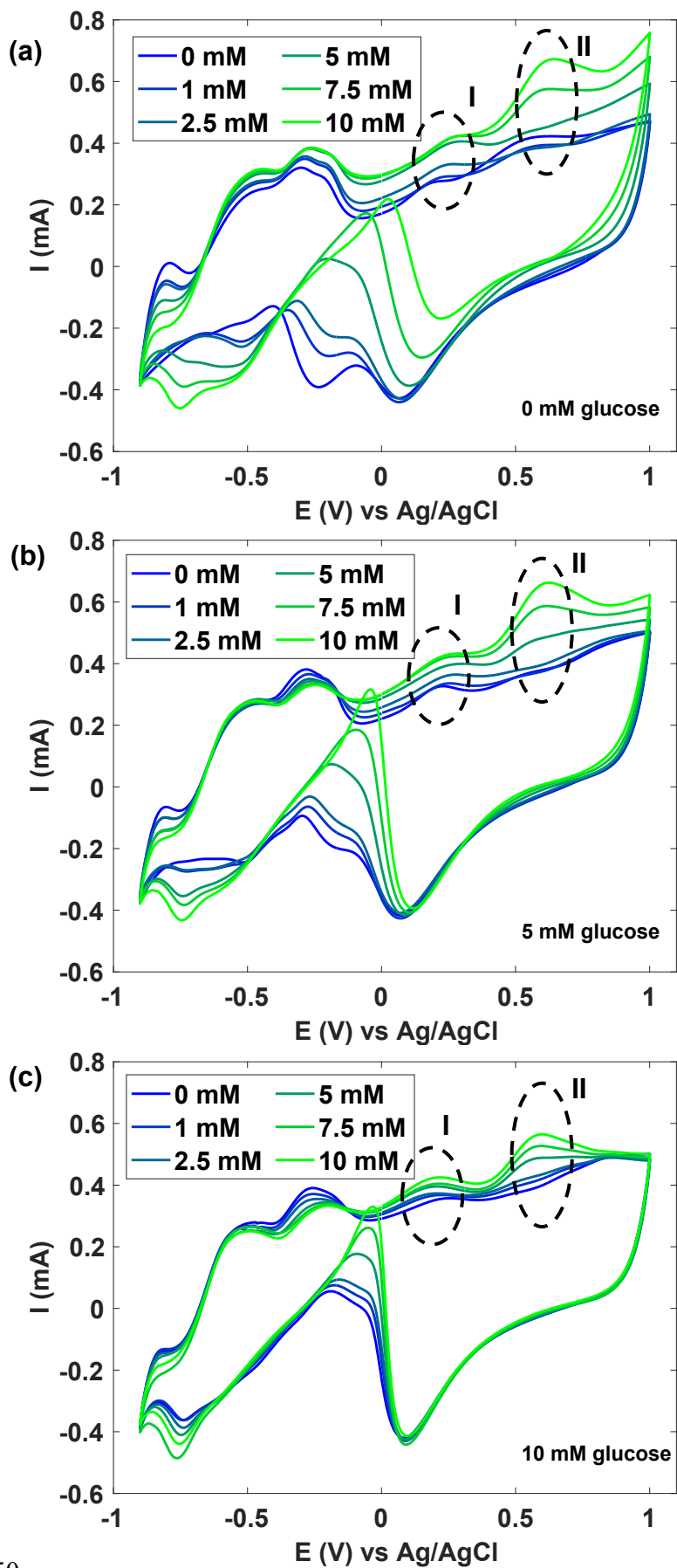


Figure 5.7: CV analysis of cross-interference analysis between glucose and ethanol in 0.1 M chloride-free PBS (pH 7). Medium containing increasing concentrations of ethanol between 0 and 10 mM and: (a) 1 mM glucose, (b) 5 mM glucose, (c) 10 mM glucose. Oxidation peaks I and II are proportional with ethanol concentrations. Scan rate: 25 mV/s.

As glucose concentration in chloride-free neutral PBS increases, the peak currents corresponding to the ethanol oxidation peaks decrease, but continue to remain visible and proportional to the ethanol concentration (peak I and II in Figure 5.7). Therefore, ethanol sensing in a neutral environment in the presence of glucose is feasible. However, the sensitivity and LoD were not thoroughly investigated in this study, therefore the conclusion remains qualitative.

5.5 Summary and contributions

This chapter describes the analysis of the performance of nanostructured Pt electrodes in a neutral solution. The key contributions of this chapter include:

- I. The evaluation of the optimal CV potential window in chloride-free neutral PBS with and without ethanol, which resulted to be between -0.9 and 1 V.
- II. The evaluation of the sensitivity and intersample LoD of the electrodes, which are respectively $145,46 \pm 7.42 \text{ uA}/(\text{mM}\cdot\text{cm}^2)$ and $849 \pm 43 \text{ uM}$.
- III. The evaluation of the influence of interferences on ethanol sensing. In particular, it was observed that the only non-negligible interferent among the ones tested was glucose. This cross-interference was therefore investigated further and results showed there is sensitivity to ethanol even at high glucose concentrations when working with voltammetric techniques.

In the next section the focus will be the analysis of the electrodes' performance in acidic environment.

Chapter 6: Sensing of ethanol in acidic environment

This subchapter presents the analysis of ethanol detection in acidic solutions. This analysis was conducted because the beer fermentation broth is characterised by an acidic pH.

6.1 Materials and methods

All experiments were performed at room temperature using an Autolab potentiostat, an external double junction Ag/AgCl RE, a Pt wire CE and the nanostructured electrodes as the WE, where not specified otherwise. The volume of solution used was 50 mL.

The 0.1 M chlorides-free neutral PBS was prepared as explained in the subchapter 5.1. To lower the pH of the medium phosphoric acid was added. The resulting buffer pH was 4. Moreover, 0.1 M PBS (with chlorides) from VWR was also used, after lowering its pH, to establish the influence of chloride ions on the electrode's performance. Ethanol solution was prepared by diluting absolute ethanol with the chloride-free neutral PBS. Glucose solution was prepared using the chloride-free neutral PBS, stored in a refrigerator, and used within three days.

CV measurements were performed to determine the optimal potential range, to qualitatively measure ethanol sensitivity, and to assess the reproducibility of the electrodes. The scan rate used was 25 mV/s.

Two different protocols were used and compared for CA measurements to identify the potential at which the electrodes exhibited the highest response to ethanol and glucose separately. In both protocols, a magnetic stirrer with a speed of 600 rpm in the first protocol and of 450rpm in the second, and a 50 mL beaker were used. The protocols were two:

- I. Spiking protocol: first, all electrodes were rinsed with DI water and dried. After, the working potential was applied for 120 seconds to allow the current to stabilize. After the stabilization, the current was recorded for 150 seconds. The current averaged in the first 40 seconds represents the baseline current, while the current averaged in the last 50 seconds represents the electrodes' response to the analyte.
- II. Continuous protocol: the electrodes were first activated in chloride-free PBS (pH 4) by performing CV at 100 mV/s for 10 cycles. Then a continuous measurement of current is done for the electrodes submerged in the solution without the analyte. The working potential was held constant for 120 s, then increased by steps of 0.1 V. The current averaged in the last 50 s at every potential tested represents the baseline current. This protocol was then repeated for electrodes submerged in the analyte-containing solution. The averaging process in this second configuration yields the current that represents the electrodes' response to the analyte. This protocol was performed using an external double junction Ag/AgCl RE containing chloride-free acidic PBS as the outer filling solution, to lower possible chloride ions leaking.

Finally, CV measurements were used to build the calibration plot in acidic solution and in the presence of glucose. Peak currents in the CV were manually determined after subtracting the baseline from each curve. The baseline was computed as the tangent to the CV scan at the minimum peak positioned between 0 and 0.2 V. The average sensitivity was evaluated using 5 freshly prepared electrodes. The standard error on the average sensitivity was computed as the ratio of the standard deviation of sensitivities to the square root of the sample size.

The LoD was computed using two methods:

- I. LoD intrasample was computed as the average of the LoD calculated for each electrode. The LoD for each electrode in each individual medium is equal to $3 \cdot Sb/s$, where Sb is the standard deviation between the peaks of the last three CV scans in the blank medium, and s is the sensitivity computed for each electrode. The error of this LoD was computed as the standard error among five electrodes, thus it is equal to the ratio between the standard deviation among the intrasample LoDs for each electrode and the square root of the number of electrodes.
- II. LoD intersample was computed as $3 \cdot \overline{Sb}/\bar{s}$, where \overline{Sb} is the standard deviation of the signals in the blank medium between all electrodes and \bar{s} is the average sensitivity. The error of this LoD coincides with the percentage standard error of the average sensitivity, which is the only influential error.

The computations were done with the Excel application.

6.2 Definition of the optimal potential window in CV

The potential range was evaluated as in the neutral environment analysis. These were performed in the chloride-free acidic PBS with and without 2.5 mM ethanol. To identify the lower potential limit, the upper limit was fixed at 1 V, and vice versa for the upper limit analysis. Limits were identified based on the visibility of the HER and OER peaks. Figures 6.1 and 6.2 respectively show the lower and upper potential limit analyses in the blank solution and in the presence of ethanol.

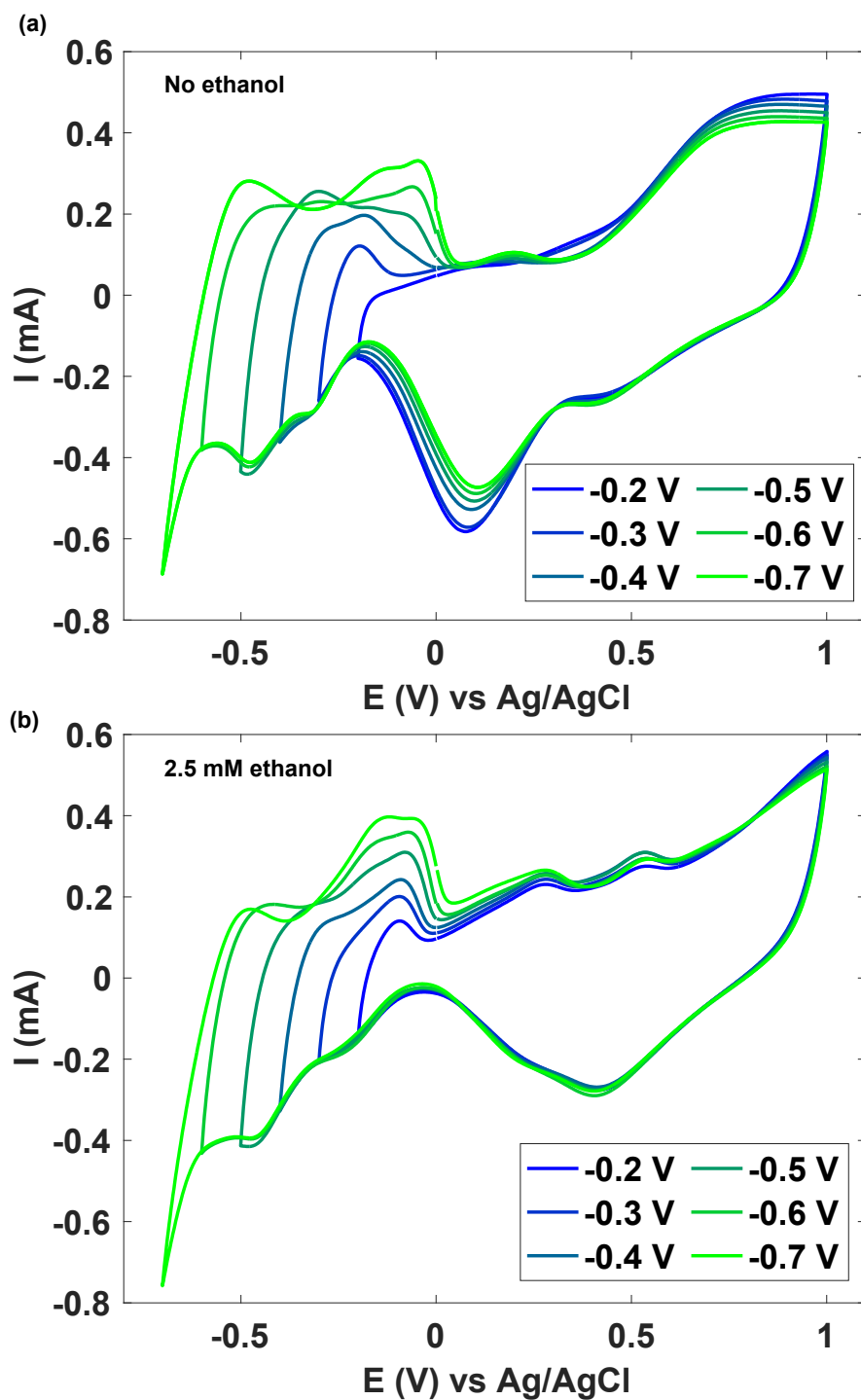


Figure 6.1: CV measurements to identify the lower potential of the window in 0.1 M chloride-free PBS (pH 4) without (a), and with 2.5 mM ethanol (b). Scan rate: 25 mV/s.

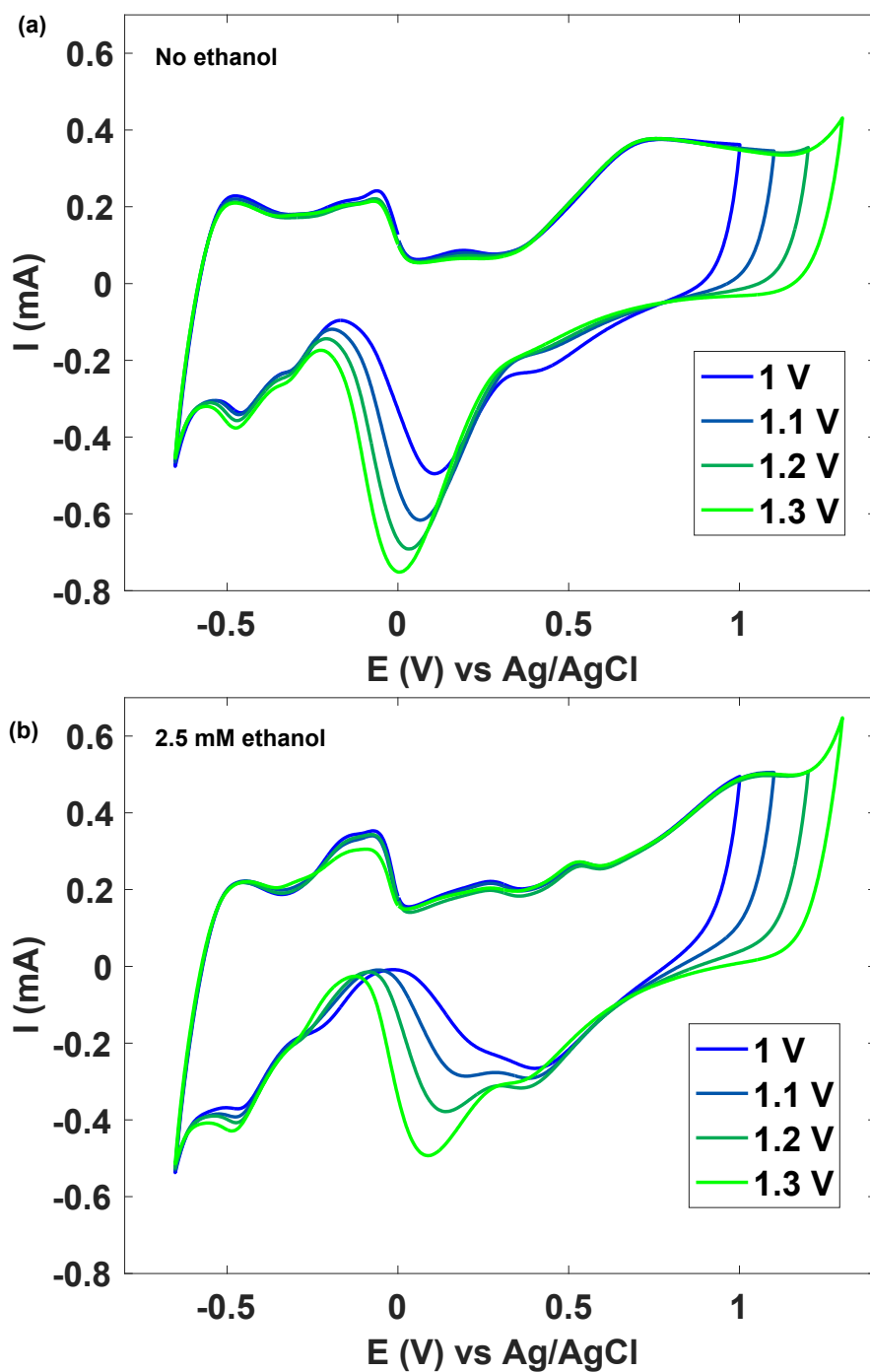


Figure 6.2: CV measurements to identify the higher potential of the window in 0.1 M chloride-free PBS (pH 4) without (a), and with 2.5 mM ethanol (b). Scan rate: 25 mV/s.

The optimal potential window determined from this analysis was between -0.65 and 1.2 V.

6.3 Identification of ethanol electrooxidation peaks in CV

Once the potential range has been selected, the ethanol sensitivity was tested qualitatively by conducting CV tests with various ethanol concentrations as shown in Figure 6.3.

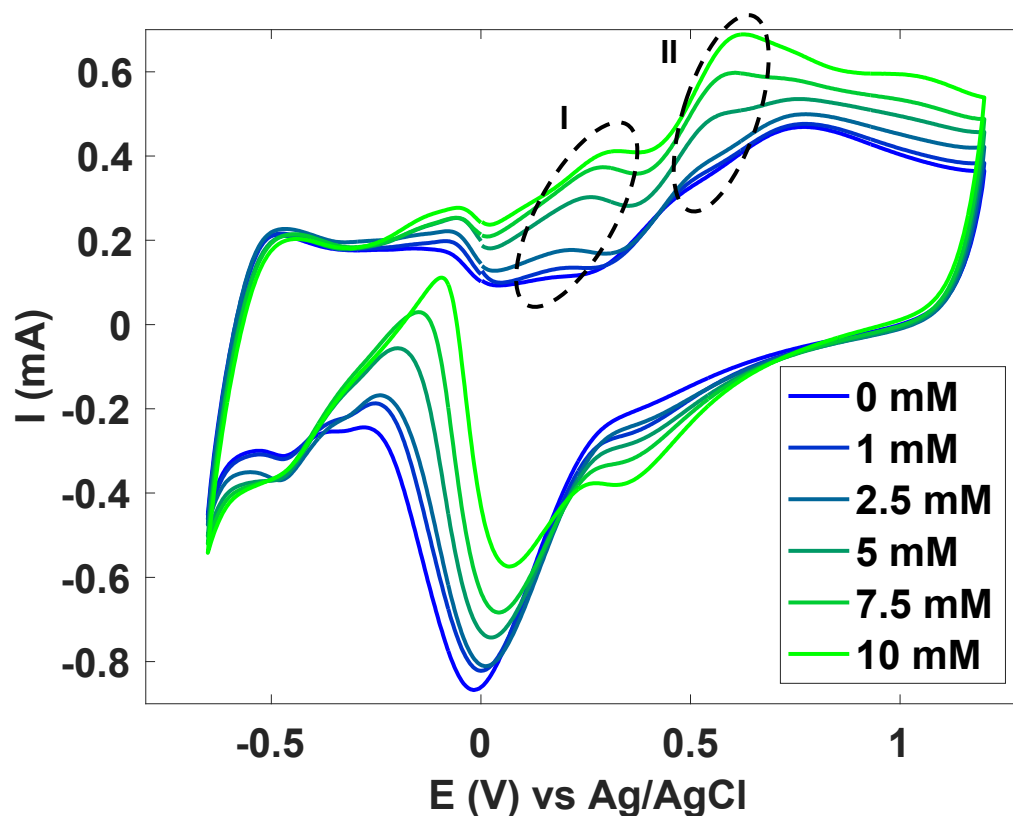


Figure 6.3: CVs acquired for different concentrations of ethanol in the range 0-10 mM at nanostructured electrodes in 0.1 M chloride-free PBS (pH 4). Oxidation peaks I) and II) are more prominent as the ethanol concentration increases. Scan rate: 25 mV/s.

As is apparent, the measured output current is proportional to the ethanol concentration. Two anodic peaks, indicated as I and II in Figure 6.3, are associated with ethanol oxidation. Detailed analysis of the reactions occurring at the different potentials would require advanced techniques like *in situ* FTIR or DEMS [48].

The sensitivity to ethanol was also tested in an acidic buffer containing chloride ions, as shown in Figure 6.4.

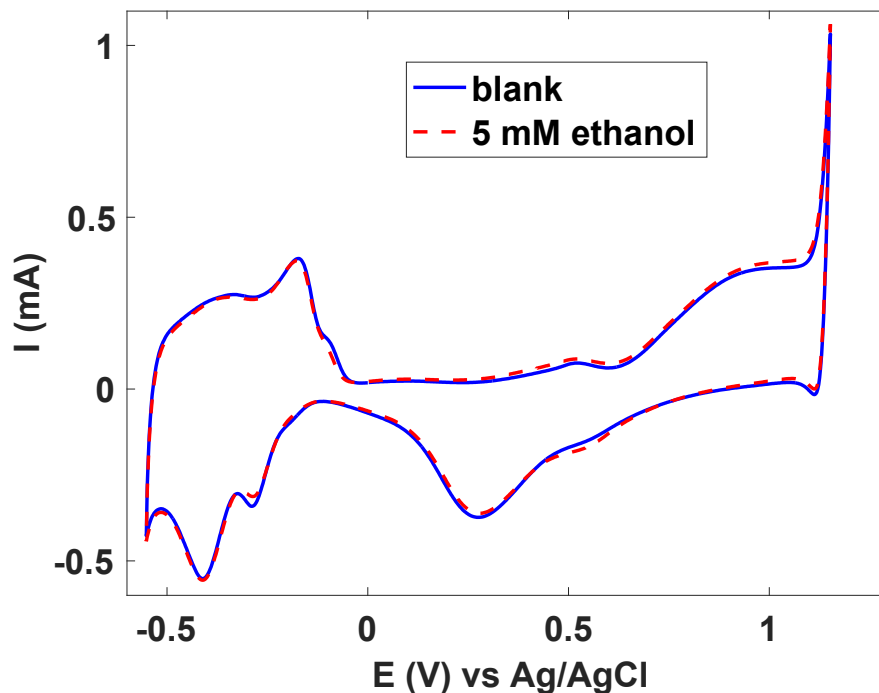


Figure 6.4: CVs in absence and presence of 5 mM ethanol in 0.1 M PBS (pH 4) in the presence of chlorides. Scan rate: 25 mV/s.

As can be observed from Figure 6.4 the optimal potential range for the acidic medium in the presence of chlorides is between -0.55 and 1.15 V. The scans in absence and presence of ethanol overlap completely, indicating that ethanol detection is not possible when chloride ions are present in solution. This is because these charged particles get adsorbed onto the catalyst surface, poisoning it, thus significantly reducing its ability to catalyse ethanol oxidation [7].

6.3.1 Glucose cross-interference with ethanol detection in CV

In alcoholic beverages, both glucose and ethanol are present. Therefore, it is essential to evaluate this cross-interference when developing ethanol sensors for beer fermentation. This test was conducted using CV, as shown in Figure 6.5.

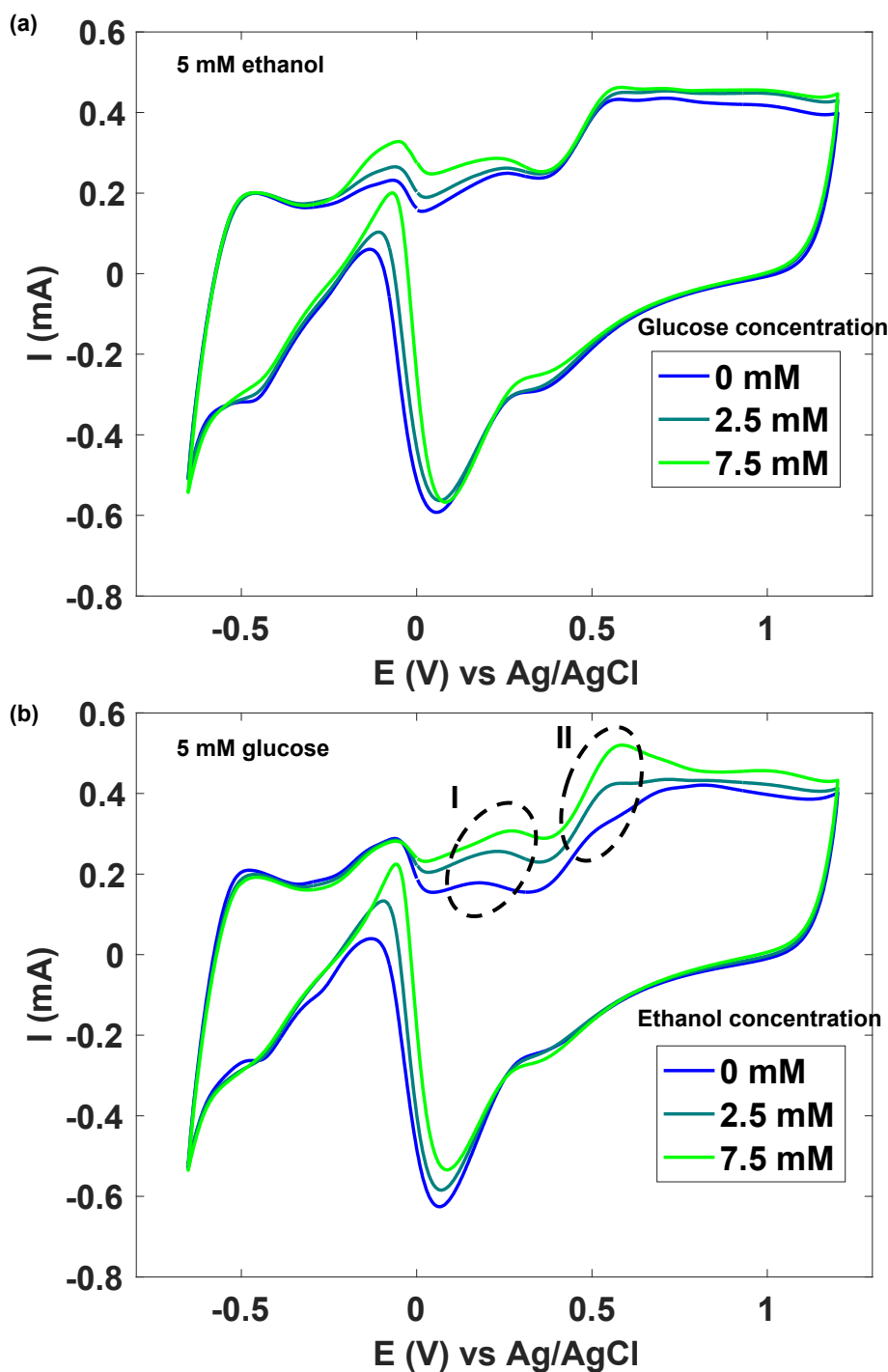


Figure 6.5: Qualitative analysis of ethanol and glucose cross interference in 0.1 M chloride-free PBS (pH 4). (a) CVs at two different concentrations of glucose (2.5 and 7.5 mM) in the presence of ethanol (5 mM). (b) CVs at two different concentrations of ethanol (2.5 and 7.5 mM) in the presence of glucose (5 mM). Peak I) and II) are representative of ethanol oxidation. Scan rate: 25 mV/s.

In the CVs for ethanol sensing in the presence of glucose, represented in Figure 6.5 (b), the two anodic peaks identified in the previous section are clearly visible, and the current peaks increase proportionally with the analyte concentration. In contrast, the CVs for glucose sensing in the presence of ethanol, represented

in Figure 6.5 (a), do not show any proportionality between output current and glucose concentration for the two mentioned peaks. These findings confirm that ethanol can be detected in acidic medium even when glucose is present. The next steps involve quantifying this ethanol detection ability by determining the sensitivity and the intersample and intrasample LoD of the sensor in the presence of different glucose concentrations.

6.4 Sensor's calibration using CA

Having established that ethanol can be sensed in acidic solution, even in the presence of glucose, the next step was to determine the potential for CA measurements to build a calibration plot. The two CA protocols were used to evaluate the electrodes' response to ethanol and glucose addition in acidic solution. The results are shown in Figure 6.6 (a) and (b).

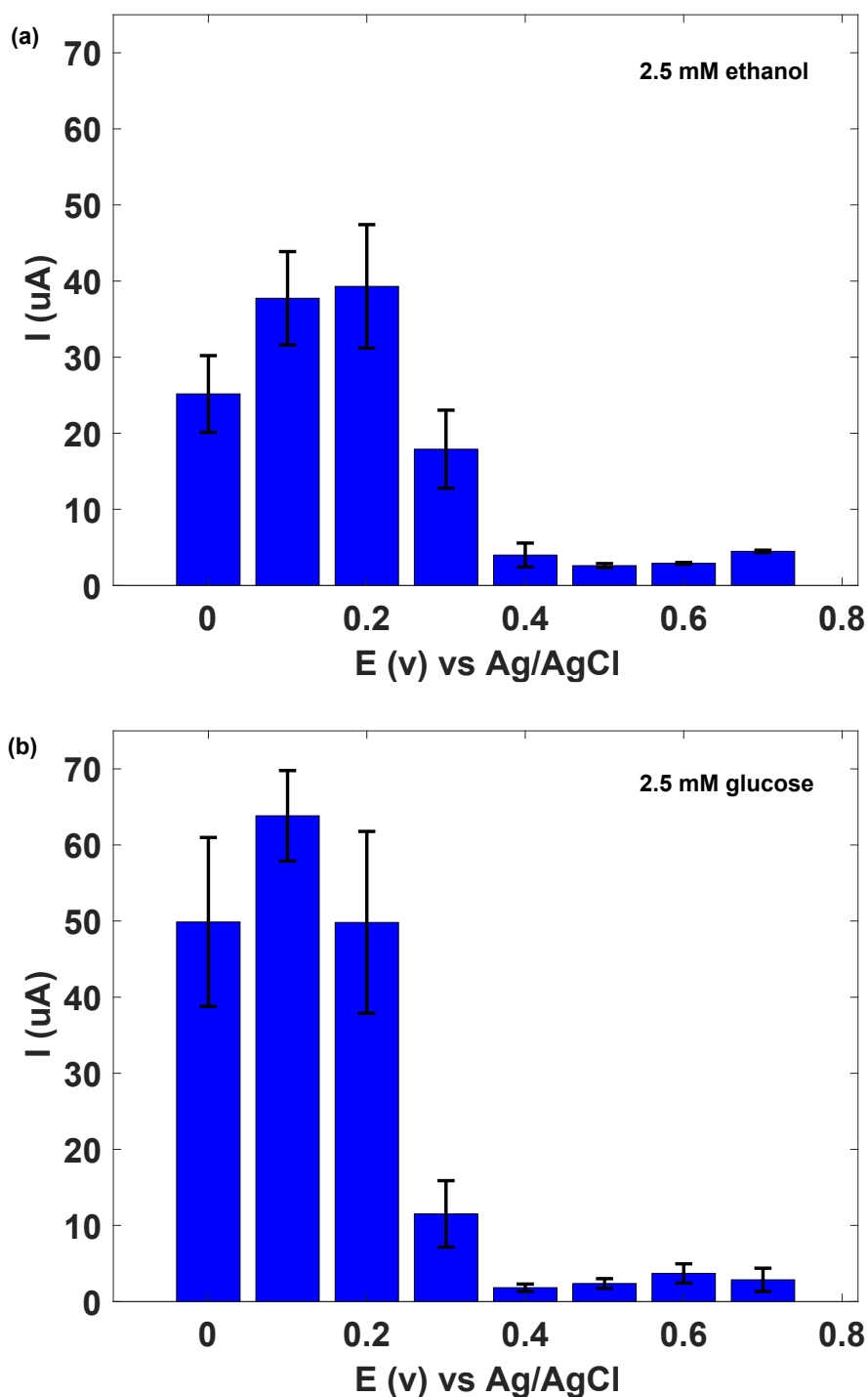


Figure 6.6: Average step current response to 2.5 mM ethanol (a) and 2.5 mM glucose (b) in 0.1 M chloride-free PBS (pH 4) at different potentials. (a) Continuous CA protocol for ethanol measurements; error bars: standard error of the step current for three electrodes. Sample size: $n=3$; stirring speed: 450 rpm. (b) Spiking CA protocol for glucose measurements; error bars: standard error of the step current for two electrodes. Sample size: $n=2$; stirring speed: 600 rpm.

The response of the electrodes to glucose and ethanol are the highest when a potential is set between 0 and 0.3 V and applied relative to Ag/AgCl RE. These results agree with the peak I that can be observed in Figures 6.3 and 6.5. The

error on the average step current was computed as the standard error among the different electrodes, thus by dividing the standard deviation of the step current among the electrodes by the square root of the number of electrodes.

The result of this analysis is that the response of glucose and ethanol happens at the same working potentials, therefore it is not possible to proceed with the construction of the calibration plot with this approach. It would, in fact, be impossible to differentiate between the oxidation of glucose molecules or ethanol ones. Thus, the calibration plot was constructed using CV, as described in the next sections.

6.5 Intra-electrode reproducibility

To ensure the reliability of the calibration constructed based on CV measurements, intra-electrode reproducibility was assessed. Figure 6.7 shows the CV scans for a single electrode, freshly prepared, used three times in chloride-free acidic PBS with 10 mM ethanol.

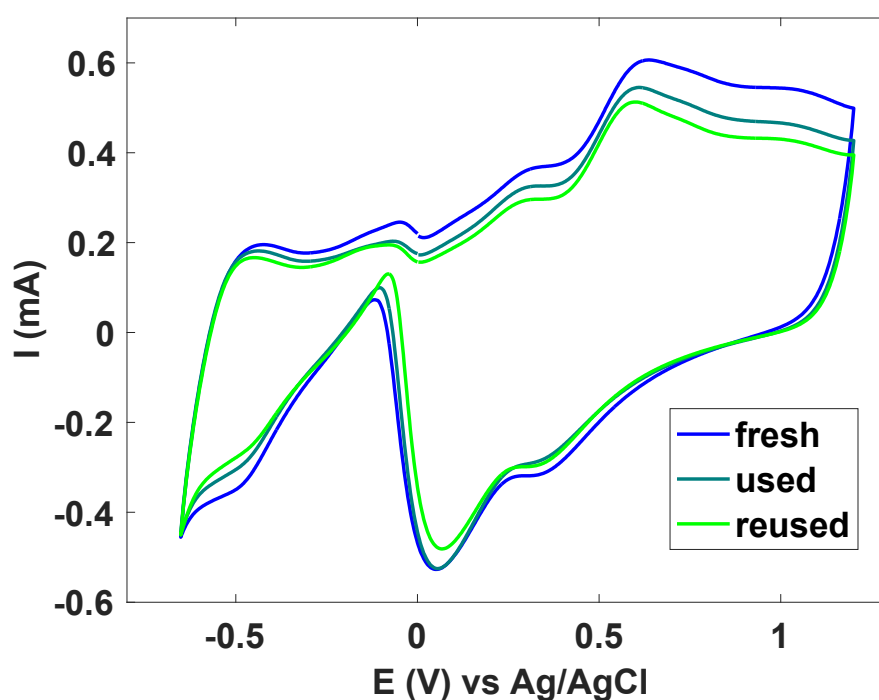


Figure 6.7: CVs in 0.1 M chloride-free PBS (pH 4) containing 10mM ethanol of the same electrode used three consecutive times. Scan rate: 25 mV/s.

The peak current of the reused electrode was lower than that of freshly prepared one, despite the characteristic peaks remain visible. This decline may be attributed to the effect of ion poisoning. For this reason, only freshly prepared electrodes were used to calibrate the sensor.

6.6 Sensor's calibration

Three different calibration plots were built to evaluate the detection ability of the electrodes in chloride-free acidic PBS in the presence of three different glucose concentrations. Two calibration plots were constructed based on the measured peak currents of the two anodic peaks identified earlier (see Section 6.3). The analysis presented here focuses only on the peak around 0.6 V, as it provides better sensitivity and reproducibility.

The obtained results demonstrate that the increasing glucose concentration reduces ethanol sensitivity (Table 6.2). Additionally, as the ethanol concentration increases, the peak potential shifts to more positive values, as shown in Figure 6.8. The linearity of the obtained plots is always higher than 0.96 (R^2).

As shown in Table 6.2, the intrasample LoD is consistently below 1 mM. However, in respect to the literature studies shown in Table 2.2 (see Chapter 2), this result is more than ten-times higher. The intersample LoD is generally higher than the intrasample parameter, due to the difference in the response offset among samples, despite similar analyte sensitivity.

Solution (glucose concentration in 0.1 M chloride-free PBS (pH 4))	Sensitivity ($\mu\text{A}/\text{mM}$)	Sensitivity per unit area ($\mu\text{A}/(\text{mM}\cdot\text{cm}^2)$)	LoD intrasample (mM)	LoD intersample (mM)
0 mM	$34,44 \pm 2,14$	274.19 ± 17.05	$0,622 \pm 0,037$	$1,13 \pm 0,07$
2.5 mM	$28,05 \pm 1,12$	223.35 ± 8.90	$0,589 \pm 0,118$	$5,694 \pm 0,227$
7.5 mM	$23,29 \pm 0,89$	185.41 ± 7.05	$0,749 \pm 0,134$	$2,213 \pm 0,084$

Table 6.1: Comparison of ethanol sensitivity and LoD in 0.1 M chloride-free PBS (pH 4)

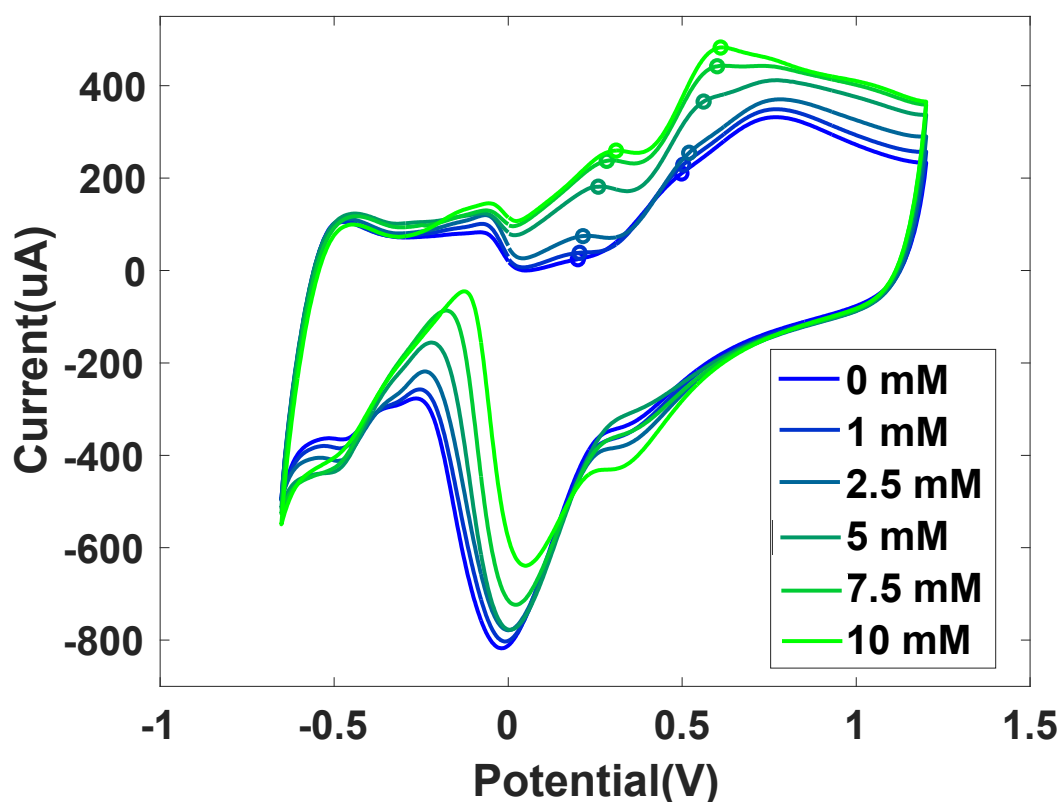


Figure 6.8: CV scans in 0.1 M chloride-free PBS (pH 4) with different ethanol concentrations after baseline subtraction. The peak currents were identified manually. Scan rate: 25 mV/s

6.7 Summary and contributions

This chapter describes the analysis of the performance of nanostructured Pt electrodes in acidic solutions. The key contributions of this chapter include:

- I. The evaluation of the optimal CV potential window in chloride-free acidic PBS with and without ethanol, which resulted to be between -0.65 and 1.2 V.
- II. The evaluation of the ethanol sensitivity and LoD in chloride-free acidic PBS containing different glucose concentrations. The highest sensitivity is obtained when the medium doesn't contain glucose, and it results in $274.19 \pm 17.05 \text{ uA}/(\text{mM}\cdot\text{cm}^2)$ with an intrasample LoD of $622 \pm 37 \text{ uM}$ and an intersample LoD of $1130 \pm 70 \text{ uM}$.

Chapter 7: Conclusion and future works

This thesis presents the development of electrochemical sensors to detect ethanol in the beer fermentation broth. The sensors were created based on Pt SPE. Two different sensor routes were exploited in this work: an enzymatic and a non-enzymatic approach.

The enzymatic sensor was developed using AOX species *Hansenula* and *Pichia Pastoris*. The immobilization of the enzyme was conducted adapting a previously implemented protocol that involves immobilizing the enzyme by crosslinking it with BSA using GA [63]. The enzyme solution was drop-cast onto the electrodes to obtain two different enzyme loadings: around 0.2 units/mm² and around 1 units/mm². Despite using two different enzyme species, the immobilization of the enzyme on the electrode did not show the expected stability, as the enzyme layer flaked off after CV tests in solution. For this reason, the sensor response to ethanol was absent.

Future experiments should focus on:

- I. Determining the influence of different amounts/concentrations of BSA, GA and enzyme on the activity of the enzyme after its integration on the electrode. More experiments can be performed by testing other enzyme species and producers.
- II. Possibly improving the electrode's performance by modifying it with the addition of electrocatalysts, mediators, enzyme stabilizers and nanostructuring strategies. All the mentioned techniques are reported in the literature.

The non-enzymatic sensor relied on the integration of Pt nanostructured layers via CC technique; the ethanol detection performance was investigated in both neutral and acidic environments. The main contributions of this research part are listed below.

- I. **Effective nanostructuring of the electrodes.** The implemented protocol was demonstrated to be reproducible and the increase of the

ESA was successful. The resulting roughness factor is equal to $119,9 \pm 0,2$. This was observed through the SEM imaging of the nanostructured samples as well as with the evaluation of the performance in ethanol detection.

- II. **Effective ethanol detection in neutral and acidic environments**, whilst in alkaline solution the response of the electrodes was absent. The calibration plot was constructed using CA and CV respectively in neutral and acidic solutions. The highest response was obtained in the acidic environment, where the sensitivity to ethanol resulted to be $274.19 \pm 17.05 \text{ uA}/(\text{mM}\cdot\text{cm}^2)$ and the intrasample and intersample LoD are equal to $622 \pm 37 \text{ uM}$ and $1130 \pm 70 \text{ uM}$ respectively.
- III. **Effective ethanol detection in the presence of glucose**. The investigation of the cross-interference between glucose and ethanol is crucial as both analytes are always present in the beer fermentation broth. In particular, the sensitivity to ethanol decreases to 81.5 % and 67.6 % in acidic solution containing 2.5 mM and 7.5 mM of glucose respectively.

Future research directions may include:

- I. **Improving the results of nanostructuring** obtained with the LSV technique. It would be valuable to compare the nanostructures produced by the LSV and the CC techniques under equivalent charge applied.
- II. Constructing **calibration plots** for ethanol detection in the presence of glucose in **neutral environment**. The analysis conducted on this topic in this work, was qualitative but demonstrated the feasibility of ethanol detection under these conditions.
- III. Developing a glucose sensor for **simultaneous ethanol and glucose detection** both in neutral and acidic environments. A glucose sensor, such as one based on glucose oxidase (GOX), could be integrated with the ethanol sensors developed in this thesis. This would enable simultaneous detection in both environments and allow the selection of the appropriate calibration plot to compute the ethanol concentration in solution.
- IV. **Understanding ethanol and glucose reactions** on the electrode's surface at different applied potentials. Techniques such as *in situ* FTIR, XPS, DEMS could provide insights into the reaction mechanisms and help identify optimal potentials for CA ethanol detection.
- V. Testing the **reusability** and the **long-term functional stability for continuous monitoring** of the electrodes in neutral and acidic environments.
- VI. Addressing ethanol **detection in the presence of chlorides**. Since beer fermentation broth contains chloride ions, poisoning could hinder the

detection of the analyte. Applying a specially developed protective membrane to repel chloride ions from the electrode surface may help mitigate this issue.

Bibliography

- [1] P. D. Thungon, A. Kakoti, L. Ngashangva, and P. Goswami, “Advances in developing rapid, reliable and portable detection systems for alcohol,” May 22, 2017, *Elsevier Ltd.* doi: 10.1016/j.bios.2017.05.041.
- [2] A. M. Azevedo, D. M. F. Prazeres, J. M. S. Cabral, and L. P. Fonseca, “Ethanol biosensors based on alcohol oxidase,” Sep. 03, 2004. doi: 10.1016/j.bios.2004.09.030.
- [3] A. S. Campbell, J. Kim, and J. Wang, “Wearable electrochemical alcohol biosensors,” Aug. 01, 2018, *Elsevier B.V.* doi: 10.1016/j.coelec.2018.05.014.
- [4] S. Maicas, “The role of yeasts in fermentation processes,” Aug. 01, 2020, *MDPI AG.* doi: 10.3390/microorganisms8081142.
- [5] O. Coskun, “Separation techniques: Chromatography,” *North Clin Istanb*, pp. 156–160, 2016, doi: 10.14744/nci.2016.32757.
- [6] J. Baranwal, B. Barse, G. Gatto, G. Broncova, and A. Kumar, “Electrochemical Sensors and Their Applications: A Review,” Sep. 01, 2022, *Multidisciplinary Digital Publishing Institute (MDPI).* doi: 10.3390/chemosensors10090363.
- [7] G. A. Naikoo *et al.*, “Recent Advances in Non-Enzymatic Glucose Sensors Based on Metal and Metal Oxide Nanostructures for Diabetes Management- A Review,” Sep. 22, 2021, *Frontiers Media S.A.* doi: 10.3389/fchem.2021.748957.
- [8] Adam Hulanicki, Stanislaw Glab, and Folke Ingman, “Chemical sensors definitions and classification,” *Pure & Appl. Chem.*, vol. 63, pp. 1247–1250, 1991.
- [9] Jorgen Vessman, Raluca I. Stefan, Jacobus F. Van Staden, and Klaus Danzer, “Selectivity in analytical chemistry,” *Pure Appl. Chem*, vol. 73, no. 8, pp. 1381–1386, 2001.
- [10] N. G. Costa, J. C. Antunes, A. J. Paleo, and A. M. Rocha, “A Review on Flexible Electrochemical Biosensors to Monitor Alcohol in Sweat,” Apr. 01, 2022, *MDPI.* doi: 10.3390/bios12040252.
- [11] T. B. Goriushkina, A. P. Soldatkin, and S. V. Dzyadevych, “Application of amperometric biosensors for analysis of ethanol, glucose, and lactate in wine,” *J Agric Food Chem*, vol. 57, no. 15, pp. 6528–6535, Aug. 2009, doi: 10.1021/jf9009087.
- [12] “repeatability,” IUPAC Compendium of Chemical Terminology. [Online]. Available: <https://doi.org/10.1351/goldbook.R05293>
- [13] “reproducibility,” IUPAC Compendium of Chemical Terminology. [Online]. Available: <https://doi.org/10.1351/goldbook.R05305>
- [14] “linear range,” IUPAC Compendium of Chemical Terminology. [Online]. Available: <https://doi.org/10.1351/goldbook.L03558>

- [15] D. Grieshaber, R. Mackenzie, J. Vörös, and E. Reimhult, “Electrochemical Biosensors-Sensor Principles and Architectures,” *Sensors*, vol. 8, pp. 1400–1458, 2008, [Online]. Available: www.mdpi.org/sensors
- [16] “Reference Electrodes,” LibreTexts. Accessed: Nov. 07, 2024. [Online]. Available: [https://chem.libretexts.org/Bookshelves/Analytical_Chemistry/Supplemental_Modules_\(Analytical_Chemistry\)/Analytical_Sciences_Digital_Library/Courseware/Analytical_Electrochemistry%3A_Potentiometry/03_Potentiometric_Theory/04_Reference_Electrodes](https://chem.libretexts.org/Bookshelves/Analytical_Chemistry/Supplemental_Modules_(Analytical_Chemistry)/Analytical_Sciences_Digital_Library/Courseware/Analytical_Electrochemistry%3A_Potentiometry/03_Potentiometric_Theory/04_Reference_Electrodes)
- [17] “Application Area: Fundamental Reference Electrodes and Their Usage,” Apr. 2019. [Online]. Available: www.metrohm.com/en/products/electrochemistry.
- [18] “Screen-printed platinum electrode - Metrohm.” Accessed: Nov. 07, 2024. [Online]. Available: <https://metrohm-dropsens.com/products/electrodes/screen-printed-electrodes/screen-printed-platinum-electrode/>
- [19] O. D. Renedo, M. A. Alonso-Lomillo, and M. J. A. Martínez, “Recent developments in the field of screen-printed electrodes and their related applications,” *Talanta*, vol. 73, no. 2, pp. 202–219, 2007, doi: <https://doi.org/10.1016/j.talanta.2007.03.050>.
- [20] Taewhan Kim *et al.*, “Applications of Voltammetry in Lithium Ion Battery Research,” *J. Electrochem. Sci. Technol*, vol. 11, no. 1, pp. 14–25, 2020, doi: [10.33961/jecst.2019.00619](https://doi.org/10.33961/jecst.2019.00619).
- [21] R. Serra-Maia *et al.*, “Mechanism and Kinetics of Hydrogen Peroxide Decomposition on Platinum Nanocatalysts,” *ACS Appl Mater Interfaces*, vol. 10, no. 25, pp. 21224–21234, Jun. 2018, doi: [10.1021/acsami.8b02345](https://doi.org/10.1021/acsami.8b02345).
- [22] M. M. Barsan and C. M. A. Brett, “An alcohol oxidase biosensor using PNR redox mediator at carbon film electrodes,” *Talanta*, vol. 74, no. 5, pp. 1505–1510, Feb. 2008, doi: [10.1016/j.talanta.2007.09.027](https://doi.org/10.1016/j.talanta.2007.09.027).
- [23] E. C. Rama, J. Biscay, M. B. González García, A. J. Reviejo, J. M. Pingarrón Carrazón, and A. Costa García, “Comparative study of different alcohol sensors based on Screen-Printed Carbon Electrodes,” *Anal Chim Acta*, vol. 728, pp. 69–76, May 2012, doi: [10.1016/j.aca.2012.03.039](https://doi.org/10.1016/j.aca.2012.03.039).
- [24] J. Biscay, E. Findlay, and L. Dennany, “Electrochemical monitoring of alcohol in sweat,” *Talanta*, vol. 224, Mar. 2021, doi: [10.1016/j.talanta.2020.121815](https://doi.org/10.1016/j.talanta.2020.121815).
- [25] M. Gamella *et al.*, “A novel non-invasive electrochemical biosensing device for in situ determination of the alcohol content in blood by monitoring ethanol in sweat,” *Anal Chim Acta*, vol. 806, pp. 1–7, Jan. 2014, doi: [10.1016/j.aca.2013.09.020](https://doi.org/10.1016/j.aca.2013.09.020).
- [26] A. G. V. De Prada, N. Peña, M. L. Mena, A. J. Reviejo, and J. M. Pingarrón, “Graphite-Teflon composite bienzyme amperometric biosensors for monitoring of alcohols,” *Biosens Bioelectron*, vol. 18, no. 10, pp. 1279–1288, 2003, doi: [10.1016/S0956-5663\(03\)00074-5](https://doi.org/10.1016/S0956-5663(03)00074-5).
- [27] J. Gonzalo-Ruiz, M. A. Alonso-Lomillo, R. Escudé-Pujol, and F. J. Muñoz, “Integrated Bienzyme Chip for Ethanol Monitoring,” *Electroanalysis*, vol. 18, no. 12, pp. 1231–1234, 2006, doi: <https://doi.org/10.1002/elan.200603526>.
- [28] A. R. Vijayakumar, E. Csoregi, A. Heller, and L. Gorton, “Alcohol biosensors based on coupled oxidase-peroxidase systems,” *Anal Chim Acta*, vol. 327, pp. 223–234, Jan. 1996.

- [29] P. Das, M. Das, S. R. Chinnadayala, I. M. Singha, and P. Goswami, "Recent advances on developing 3rd generation enzyme electrode for biosensor applications," *Biosens Bioelectron*, vol. 79, pp. 386–397, 2016, doi: <https://doi.org/10.1016/j.bios.2015.12.055>.
- [30] M. Boujtita, J. P. Hart, and R. Pittson, "Development of a disposable ethanol biosensor based on a chemically modified screen-printed electrode coated with alcohol oxidase for the analysis of beer," 2000. [Online]. Available: www.elsevier.com/locate/bios
- [31] D. Farina *et al.*, "Development of a biosensor telemetry system for monitoring fermentation in craft breweries," *Food Chem*, vol. 218, pp. 479–486, Mar. 2017, doi: [10.1016/j.foodchem.2016.09.092](https://doi.org/10.1016/j.foodchem.2016.09.092).
- [32] D. Carelli, D. Centonze, A. De Giglio, M. Quinto, and P. G. Zambonin, "An interference-free first generation alcohol biosensor based on a gold electrode modified by an overoxidised non-conducting polypyrrole film," *Anal Chim Acta*, vol. 565, no. 1, pp. 27–35, Apr. 2006, doi: [10.1016/j.aca.2006.02.023](https://doi.org/10.1016/j.aca.2006.02.023).
- [33] S. Piermarini, G. Volpe, M. Esti, M. Simonetti, and G. Palleschi, "Real time monitoring of alcoholic fermentation with low-cost amperometric biosensors," *Food Chem*, vol. 127, no. 2, pp. 749–754, Jul. 2011, doi: [10.1016/j.foodchem.2011.01.008](https://doi.org/10.1016/j.foodchem.2011.01.008).
- [34] S. R. Chinnadayala, M. Santhosh, N. K. Singh, and P. Goswami, "Alcohol oxidase protein mediated in-situ synthesized and stabilized gold nanoparticles for developing amperometric alcohol biosensor," *Biosens Bioelectron*, vol. 69, pp. 155–161, Jul. 2015, doi: [10.1016/j.bios.2015.02.015](https://doi.org/10.1016/j.bios.2015.02.015).
- [35] Ö. Türkarslan, A. E. Böyükbayram, and L. Toppare, "Amperometric alcohol biosensors based on conducting polymers: Polypyrrole, poly(3,4-ethylenedioxythiophene) and poly(3,4-ethylenedioxyppyrrrole)," *Synth Met*, vol. 160, no. 7–8, pp. 808–813, Apr. 2010, doi: [10.1016/j.synthmet.2010.01.027](https://doi.org/10.1016/j.synthmet.2010.01.027).
- [36] J. Aymerich *et al.*, "Cost-effective smartphone-based reconfigurable electrochemical instrument for alcohol determination in whole blood samples," *Biosens Bioelectron*, vol. 117, pp. 736–742, Oct. 2018, doi: [10.1016/j.bios.2018.06.044](https://doi.org/10.1016/j.bios.2018.06.044).
- [37] G. Rocchitta *et al.*, "Enzyme biosensors for biomedical applications: Strategies for safeguarding analytical performances in biological fluids," Jun. 01, 2016, *MDPI AG*. doi: [10.3390/s16060780](https://doi.org/10.3390/s16060780).
- [38] N. G. Patel, S. Meier, K. Cammann, and G.-C. Chemnitz, "Screen-printed biosensors using different alcohol oxidases," *Sensors and Actuators*, no. 75, pp. 101–110, 2001.
- [39] G. Wen, Y. Zhang, S. Shuang, C. Dong, and M. M. F. Choi, "Application of a biosensor for monitoring of ethanol," *Biosens Bioelectron*, vol. 23, no. 1, pp. 121–129, Aug. 2007, doi: [10.1016/j.bios.2007.03.024](https://doi.org/10.1016/j.bios.2007.03.024).
- [40] Y. Wang, S. Zou, and W. Bin Cai, "Recent advances on electro-oxidation of ethanol on Pt- and Pd-based catalysts: From reaction mechanisms to catalytic materials," Sep. 02, 2015, *MDPI*. doi: [10.3390/catal5031507](https://doi.org/10.3390/catal5031507).
- [41] G. A. Camara and T. Iwasita, "Parallel pathways of ethanol oxidation: The effect of ethanol concentration," *Journal of Electroanalytical Chemistry*, vol. 578, no. 2, pp. 315–321, May 2005, doi: [10.1016/j.jelechem.2005.01.013](https://doi.org/10.1016/j.jelechem.2005.01.013).

- [42] S. C. S. Lai *et al.*, “Effects of electrolyte pH and composition on the ethanol electro-oxidation reaction,” *Catal Today*, vol. 154, no. 1–2, pp. 92–104, Sep. 2010, doi: 10.1016/j.cattod.2010.01.060.
- [43] H. A. Asiri and A. B. Anderson, “Mechanisms for Ethanol Electrooxidation on Pt(111) and Adsorption Bond Strengths Defining an Ideal Catalyst,” *J Electrochem Soc*, vol. 162, no. 1, pp. F115–F122, 2015, doi: 10.1149/2.0781501jes.
- [44] H.-F. Wang and Z.-P. Liu, “Comprehensive Mechanism and Structure-Sensitivity of Ethanol Oxidation on Platinum: New Transition-State Searching Method for Resolving the Complex Reaction Network,” *J Am Chem Soc*, vol. 130, no. 33, pp. 10996–11004, Aug. 2008, doi: 10.1021/ja801648h.
- [45] A. S. Pushkarev *et al.*, “Pt/c and Pt/SnOx/C catalysts for ethanol electrooxidation: Rotating disk electrode study,” *Catalysts*, vol. 9, no. 3, Mar. 2019, doi: 10.3390/catal9030271.
- [46] Z. B. Wang, G. P. Yin, J. Zhang, Y. C. Sun, and P. F. Shi, “Investigation of ethanol electrooxidation on a Pt-Ru-Ni/C catalyst for a direct ethanol fuel cell,” *J Power Sources*, vol. 160, no. 1, pp. 37–43, Sep. 2006, doi: 10.1016/j.jpowsour.2006.01.021.
- [47] J. Tayal, B. Rawat, and S. Basu, “Effect of addition of rhenium to Pt-based anode catalysts in electro-oxidation of ethanol in direct ethanol PEM fuel cell,” in *International Journal of Hydrogen Energy*, Mar. 2012, pp. 4597–4605. doi: 10.1016/j.ijhydene.2011.05.188.
- [48] A. Bach Delpuech, F. Maillard, M. Chatenet, P. Soudant, and C. Cremers, “Ethanol oxidation reaction (EOR) investigation on Pt/C, Rh/C, and Pt-based bi- and tri-metallic electrocatalysts: A DEMS and in situ FTIR study,” *Appl Catal B*, vol. 181, pp. 672–680, Feb. 2016, doi: 10.1016/j.apcatb.2015.08.041.
- [49] F. Criscuolo *et al.*, “Fast procedures for the electrodeposition of platinum nanostructures on miniaturized electrodes for improved ion sensing,” *Sensors (Switzerland)*, vol. 19, no. 10, May 2019, doi: 10.3390/s19102260.
- [50] I. Taurino, G. Sanz , F. Mazzei, G. Favero, G. De Micheli, and S. Carrara, “Fast synthesis of platinum nanopetals and nanospheres for highly-sensitive non-enzymatic detection of glucose and selective sensing of ions,” *Sci Rep*, vol. 5, Oct. 2015, doi: 10.1038/srep15277.
- [51] S. Ruiz-G mez, C. Fern ndez-Gonz lez, and L. Perez, “Electrodeposition as a Tool for Nanostructuring Magnetic Materials,” *Micromachines (Basel)*, vol. 13, no. 8, 2022, doi: 10.3390/mi13081223.
- [52] A. Hajian *et al.*, “Nanostructured Flower like Pt-Ru for Ethanol Oxidation and Determination,” *J Electrochem Soc*, vol. 162, no. 1, pp. B41–B46, 2015, doi: 10.1149/2.1121501jes.
- [53] F. Xu, L. Yang, F. Zhao, and B. Zeng, “Electrochemical Preparation of Porous PtCu Alloy on an Ionic Liquid Functionalized Graphene Film for the Electrocatalytic Oxidation and Amperometric Detection of Ethanol,” 2016. [Online]. Available: www.electrochemsci.org
- [54] K. Jin, F. He, and Q. Xie, “Electrocatalytic oxidation and detection of ethanol on an electroplated Pt/3D honeycomb-like nano-Au/Au disk electrode,” *Journal of Electroanalytical Chemistry*, vol. 849, Sep. 2019, doi: 10.1016/j.jelechem.2019.113375.

- [55] F. Xiao, F. Zhao, J. Zeng, and B. Zeng, “Novel alcohol sensor based on PtRuNi ternary alloy nanoparticles-multi-walled carbon nanotube-ionic liquid composite coated electrode,” *Electrochem commun*, vol. 11, no. 7, pp. 1550–1553, Jul. 2009, doi: 10.1016/j.elecom.2009.05.060.
- [56] J. Wang *et al.*, “MoS₂ nanoflower supported Pt nanoparticle as an efficient electrocatalyst for ethanol oxidation reaction,” *Int J Hydrogen Energy*, vol. 44, no. 31, pp. 16411–16423, Jun. 2019, doi: 10.1016/j.ijhydene.2019.04.251.
- [57] J. Wan, X. Ma, L. Xing, and G. Yin, “The Nonenzyme Ethanol Sensor Based on Pt NPs and Fe₃O₄ MNPs Modified Au Electrode,” 2013.
- [58] C. Xu, Y. Liu, F. Su, A. Liu, and H. Qiu, “Nanoporous PtAg and PtCu alloys with hollow ligaments for enhanced electrocatalysis and glucose biosensing,” *Biosens Bioelectron*, vol. 27, no. 1, pp. 160–166, Sep. 2011, doi: 10.1016/j.bios.2011.06.036.
- [59] C. Xu, F. Sun, H. Gao, and J. Wang, “Nanoporous platinum-cobalt alloy for electrochemical sensing for ethanol, hydrogen peroxide, and glucose,” *Anal Chim Acta*, vol. 780, pp. 20–27, May 2013, doi: 10.1016/j.aca.2013.03.068.
- [60] C. Xu, J. Wang, and J. Zhou, “Nanoporous PtNi alloy as an electrochemical sensor for ethanol and H₂O₂,” *Sens Actuators B Chem*, vol. 182, pp. 408–415, 2013, doi: 10.1016/j.snb.2013.03.035.
- [61] M. M. Pereira Silva Neves *et al.*, “A non-enzymatic ethanol sensor based on a nanostructured catalytic disposable electrode,” *Analytical Methods*, vol. 9, no. 35, pp. 5108–5114, Sep. 2017, doi: 10.1039/c7ay01078h.
- [62] R. COUDERC and J. BARATTI, “Oxidation of Methanol by the Yeast, *Pichia pastoris*. Purification and Properties of the Alcohol Oxidase,” *Agric Biol Chem*, vol. 44, no. 10, pp. 2279–2289, 1980, doi: 10.1271/bbb1961.44.2279.
- [63] N. I. Rusli, P. L. Espinar, F. Ceysens, I. Taurino, and M. Kraft, “Miniaturized Electrochemical Device for In-Situ Monitoring of Glucose, Lactate, Dissolved Oxygen, PH, and Temperature in Yeast Culture,” in *21st International Conference on Solid-State Sensors, Actuators and Microsystems, TRANSDUCERS 2021*, Institute of Electrical and Electronics Engineers Inc., Jun. 2021, pp. 188–191. doi: 10.1109/Transducers50396.2021.9495611.
- [64] J. Mascarell and M. Ryan, “Technical aspects of enzyme utilization: Dry vs liquid enzymes,” in *Feed manufacturing in Southern Europe: New challenges*, vol. 26, P. Morand-Fehr, Ed., in Cahiers Options Méditerranéennes, vol. 26. , Zaragoza : CIHEAM, 1997, pp. 161–174. [Online]. Available: <http://om.ciheam.org/om/pdf/c26/97605982.pdf>
- [65] “*Hansenula* sp. Alcohol Oxidase - Creative Biogene (n.d.)” Accessed: Nov. 20, 2024. [Online]. Available: <https://www.microbialtec.com/hansenula-sp-alcohol-oxidase-item-9285.html>
- [66] F. Largeaud, K. B. Kokoh, B. Beden, and C. Lamy, “On the electrochemical reactivity of anomers: electrocatalytic oxidation of LX-and P-D-glucose on platinum electrodes in acid and basic media,” 1995.